Implementation of HDG method for 2D anisotropic poroelastic first-order harmonic equations

Hélène Barucq, Julien Diaz, Rose-Cloé Meyer, Ha Pham

Implementation of HDG method for 2D anisotropic poroelastic first-order harmonic equations.

Hélène Barucq, Julien Diaz, Rose-Cloé Meyer, Ha Pham

RESEARCH REPORT
N° 9326
February 2020
Project-Team Magique 3D

ISSN 0249-6399 ISRN INRIA/RR--9326--FR+ENG

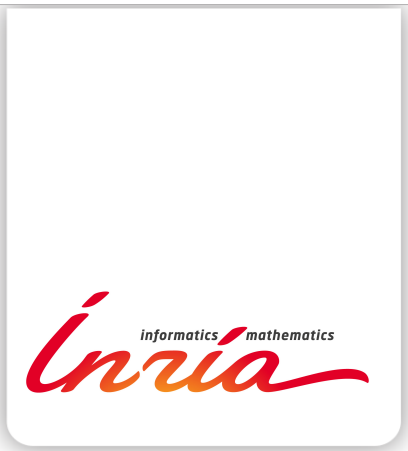

Implementation of HDG method for 2D anisotropic poroelastic first-order harmonic equations.

Hélène Barucq*, Julien Diaz*, Rose-Cloé Meyer*, Ha Pham*

Project-Team Magique 3D

Research Report n° 9326 — February 2020 — 27 pages

Abstract: In this report, we develop a Hybridizable Discontinuous Galerkin (HDG) method applied to solving the two-dimensional anisotropic poroelastic equations written as a first-order system in the frequency domain. We motivate the choice of the HDG method by the complexity of the considered equations and the high number of unknowns. The HDG method possesses indeed all the advantages of Discontinuous Galerkin method (hp-adaptivity, accuracy, ability to model rugged domain,...) without its main drawback, the dramatic increase of the number of degrees of freedom. We illustrate the accuracy of the proposed solution methodology thanks to numerical experiments and comparisons with analytical solutions that were developed in another work. We also offer numerical implementations on realistic geophysical media.

Key-words: anisotropic poroelasticity, harmonic domain, HDG method.

* Inria Bordeaux Sud-Ouest, Project-Team Magique 3D, Université de Pau et des pays de l'Adour, France

RESEARCH CENTRE
BORDEAUX – SUD-OUEST

200 avenue de la Vieille Tour
33405 Talence Cedex

Implémentation d'une méthode HD pour les équations poroélastiques anisotropes en deux dimensions dans le domaine harmonique.

Résumé : Ce rapport présente le développement d'une méthode Galerkin Discontinue Hybride (HDG) appliquée aux équations poroélastiques anisotropes en deux dimensions écrites au premier ordre dans le domaine fréquentiel. Nous expliquons le choix de la méthode HDG par la complexité des équations considérées et le nombre élevé d'inconnues. Cette méthode possède en effet tous les avantages de la méthode Galerkin Discontinue (hp-adaptivité, précision, capacité modéliser des domaines complexes...) sans son principal inconvénient, l'augmentation du nombre de degrés de liberté. Nous illustrons la précision de la méthode proposée grâce à des tests numériques et des comparaisons avec des solutions analytiques qui ont été développées dans un autre travail, sur des milieux géophysiques ralistes.

Mots-clés : poroélasticité anisotrope, domaine harmonique, méthode HDG.

1 Introduction

The numerical solution of wave propagation in poroelastic media is of great interest for many applications like subsurface exploration, vibroacoustics, biomechanics, engineering, medicine etc. In simplified models, the layers in Earth subsurface are considered as acoustic or elastic media, however to capture the attenuation phenomenon and the existence of a third wave speed, the poroelastic model is used. On the other hand, for applications in medicine, cancellous bones are also modeled as poroelastic media, see [19]. These media, which are characterized as having an elastic solid frame and pores filled with fluid, are complex and the waves propagating through them are difficult to reproduce accurately. The propagation of waves in poroelastic media has been modeled by Biot as part of the consolidation theory in [2, 3]. It has been used in a lot of works on poroelasticity, as for example [4, 8], and their references therein. In order to improve simulations, it is interesting to use discontinuous finite element methods [12] which are both very flexible and able to take into account the potentially large discontinuities in the physical parameters.

The work we present in this report is one of the pillars of the E2S-UPPA CHICkPEA project which deals with the characterization of porous conducting media from wave measurements. The idea behind this project is to provide a numerical and experimental technology capable of identifying very fine discontinuities that are invisible to seismic waves but visible by electromagnetic waves. As far as numerical contributions of CHICkPEA are concerned, the final objective is to develop a propagation code that couples the poroelastic wave equations to electromagnetism equations following the model developed by Steve Pride [28, 20, 29]. To the best of our knowledge, there are only very few works dedicated to the discretization by finite elements of the Pride model. In fact, the works that are close to this objective such as [16, 17, 18, 7, 36] reconstruct partially the electromagnetic field, or [22] where Maxwell's equations are set in a quasi-static regime. The common feature of these two works is the use of a simplified model. Indeed, solving the complete model in the temporal domain is quite a challenge because, on the one hand, the problem involves very different scales and, on the other hand, the coupling term is written as a convolution kernel whose processing requires important computational efforts. We therefore decided to work in the frequency domain where the coupling term is easily integrated, bearing in mind, however, that the multi-scale nature of the problem will have to be taken into account at some point. We present in this report the numerical method that has been developed to solve first the wave equations in a poroelastic medium before considering the coupling of elastic with electromagnetic waves.

The frequency domain is well adapted to the use of a Hybridizable Discontinuous Galerkin (HDG) method, which generates significantly lower computational costs than a standard DG method. In terms of numerical simulations, a wide variety of numerical methods has been applied to reproduce the wave propagation in poroelastic materials, like Finite Volume Method in [24], Boundary Element Method (BEM) in [31], finite differences in [37] or Finite Element Method (FEM) [32]. Spectral-element methods for poroelasticity have also been developed in [14, 27] and have demonstrated a clear efficiency in the time-domain, when based on hexahedral meshes. However, tetrahedral cells turns out to be more interesting for rugged propapagation domain, e.g., when the topography profile of the propagation domain varies strongly.

Then, Discontinuous Galerkin (DG) methods, which had initially been developed to solve fluid mechanics problems, began to be applied for wave propagation in heterogeneous media, both in time or frequency domain as in Dazel [10] and Dupuy [13] in frequency domain, and Ward [35], de la Puente [30], Li [26], or Shukla [33] in time-domain. DG methods have actually many advantages: they have good performance on unstructured and irregular meshes thanks to the use of *hp* adaptivity, they are easily parallelizable as well as the elements communicate only with their direct neighbours. The latter property is also a good point in favor of using high-order approximations since the stencil of the discrete matrix does not change when the order increases. However, the use of discontinuous basis functions results in a significant increase in the number of degrees of freedom, such that the size of the overall discrete system is much larger than that of the system associated with a continuous finite element method. This is a real disadvantage when working in the frequency domain as one can easily reach the limits of the direct solvers available in open-source that are essential to solve the problem. We can then think about using an iterative solver but in the context of our project, we are more interested in a direct solver because we have in mind to use our code to solve an inverse problem involving several second members. Then, HDG methods offer an opportunity to mitigate this drawback as displayed in the two seminal papers [9, 34]. An HDG formulation consists in reducing the discrete problem to a problem set only on the skeleton of the mesh, the original solution being reconstructed a posteriori for negligible computational costs, cell by cell. The size of the system to be inverted is thus considerably reduced, and this technique has been successfully developed for many problems, as for example in [25] for electromagnetism, or in [5, 6] for seismic waves in the harmonic regime.

Regarding waves in poroelastic media, two recent works by Fu [15] and Hungria [21] consider poroelastic wave

equations in the time domain with an HDG method. However, the first one chooses to work with the second-order poroelastic equations on the solid velocity and the fluid pressure, while we consider the first order because of our interest in the stresses in the media. The formulation of the second one is based on a different unknown (the pressure flux variable) instead of using the relative fluid velocity. Moreover, they express the transmission conditions of the method with two stabilization parameters, while we use four of them, see Section 3.2.

What we have achieved with this work is an accurate implementation of high-order HDG on realistic geophysical media. In addition to the added difficulty due to the complexity of the equations, in order to maintain numerical execution on these type of media, this requires careful choosing of appropriate characteristic values for the material parameters, so that the components of the discretized terms are balanced. An other important thing in implementation of HDG is the choice of penalization parameters. We have carried out numerical tests in order to determine the optimal values of the parameters. Our conclusion is that all the terms should be penalized.

In this report, we develop a HDG method applied to solving the two-dimensional anisotropic poroelastic equations written as a first-order system in the frequency domain. The report is organized as follows. First, we briefly introduce in Section 2 the poroelastic wave equations, which involve a large number of parameters that need to be defined. We take this opportunity to specify different examples of media that will later be used for numerical experiences. Then, we present the HDG formulation in Section 3 and the associated discretization in Section 4. Finally, Section 5 describes some numerical experiments that have been carried out to validate the method. The results are calibrated using analytical solutions that were developed in another work [1].

2 Equations

In this section, we present the anisotropic poroelastic harmonic wave equations in two dimensions, and the porous physical parameters, including the numerical values of the parameters used for the numerical tests. A poroelastic medium is composed of a solid frame, with pores filled with a fluid. Following Biot's model [3], in the frequency domain formulation, the poroelastic unknowns are the following quantities:

- $\mathbf{u}$ the frame velocity,
- $\mathbf{w}$ the relative fluid velocity,
- p the fluid pressure,
- $\boldsymbol{\tau}$ the solid stress tensor.

We also define the strain tensor $\boldsymbol{\epsilon} = \boldsymbol{\epsilon}_{\mathrm{fr}} := \dfrac{\nabla\mathbf{u} + (\nabla\mathbf{u})^t}{2}$.

2.1 First-order harmonic equations

We consider the time derivative as $\partial_t = \mathrm{i}\omega$. The poroelastic unknowns $(\mathbf{u}\,,\,\mathbf{w}\,,\,\boldsymbol{\tau}\,,\,\mathrm{p}\,)$ in first-order formulation solve the sytem

$$\begin{cases} \mathrm{i}\omega\rho_a\mathbf{u} + \mathrm{i}\omega\rho_f\,\mathbf{w} &= \nabla\cdot\boldsymbol{\tau} + \mathbf{f}_u\,, \\ \mathrm{i}\omega\rho_f\mathbf{u} + \mathrm{i}\omega\rho_{\mathrm{dyn}}\,\mathbf{w} &= -\nabla\mathrm{p} + \mathbf{f}_w\,, \\ \mathrm{i}\omega\boldsymbol{\tau} + \mathrm{i}\omega\,\boldsymbol{\alpha}\mathrm{p} &= \mathbf{C}_{\mathrm{fr}}\,\boldsymbol{\epsilon}(\mathbf{u})\,, \\ \mathrm{i}\omega\,\mathrm{p} &= -M\nabla\cdot\mathbf{w} - M\boldsymbol{\alpha} : \boldsymbol{\epsilon}(\mathbf{u})\,. \end{cases} \tag{1}$$

coupled with boundary conditions detailled in section 2.3. The physical parameters are ρ_a the averaged density in kg.m^{-3}, ρ_f the fluid density in kg.m^{-3}, $\mathbf{C}_{\mathrm{fr}}$ the stiffness matrix in Pa, $\boldsymbol{\alpha}$ the effective-stress coefficient in Pa, M the fluid-solid coupling modulus in Pa, $\rho_{\mathrm{dyn}} = \dfrac{\mathrm{i}\,\eta}{\omega\,k(\omega)}$ the dynamic density in kg.m^{-3}, with η being the viscosity of the fluid in $Pa.s$ and k the permability in m^2, and $\mathbf{f}_u$, $\mathbf{f}_w$ external forces.

Remark 1. The operation : denotes the tensorial scalar product. This means $\boldsymbol{a} : \boldsymbol{b} = \sum_{i,j} a_{ij}\,b_{ij}$.

2.2 Nondimensionalization of the equations

For the numerical implementation, the parameters may have different orders of magnitude. To manipulate numbers with a similar order of magnitude, we write the system (1) with no sources as dimensionless equations. We write $X = X_0\overline{X}$ for all the terms of the equations with X_0 a characteristic unit of measure. We assume that all bulk modulus and components of $\mathbf{C}$ are written as $\mathrm{k}_\bullet = C_0\overline{\mathrm{k}_\bullet}$. Hence, $M = C_0\overline{M}$ and $\alpha_0 = 1$. The porosity $\phi = \dfrac{V_f}{V_T}$ is considered as a ratio with no characteristic unit. We assume that ρ_a, ρ_{dyn}, ρ_f and ρ_s have the same characteristic unit ρ_0. The characteristic frequency has the same characteristic unit as ω. The system (1) with physical parameters becomes:

$$\begin{cases} \mathrm{i}\,\omega_0\,\overline{\omega}\,\rho_0\,\overline{\rho_a}\,\mathrm{u}_0\,\overline{\mathbf{u}} + \mathrm{i}\,\omega_0\,\overline{\omega}\,\rho_0\,\overline{\rho_f}\,\mathrm{w}_0\,\overline{\mathbf{w}} = \dfrac{\tau_0}{x_0}\,\nabla\cdot\,\overline{\boldsymbol{\tau}}\,, \\ \mathrm{i}\,\omega_0\overline{\omega}\,\rho_0\overline{\rho_f}\,\mathrm{u}_0\,\overline{\mathbf{u}} + \mathrm{i}\,\omega_0\overline{\omega}\,\rho_0\,\overline{\rho_{\mathrm{dyn}}}\,\mathrm{w}_0\,\overline{\mathbf{w}} = -\dfrac{\mathrm{p}_0}{x_0}\,\nabla\overline{\mathrm{p}}\,, \\ \mathrm{i}\,\omega_0\,\overline{\omega}\,\tau_0\,\overline{\boldsymbol{\tau}} + \mathrm{i}\,\omega_0\,\overline{\omega}\alpha_0\,\overline{\boldsymbol{\alpha}}\mathrm{p}_0\,\overline{\mathrm{p}}\mathbf{Id} = \dfrac{C_0\mathbf{u}_0}{x_0}\,\overline{\mathbf{C}}\,\boldsymbol{\epsilon}(\overline{\mathbf{u}})\,, \\ \mathrm{i}\,\omega_0\,\overline{\omega}\,\mathrm{p}_0\,\overline{\mathrm{p}} = -\dfrac{C_0\mathrm{w}_0}{x_0}\,\overline{M}\nabla\cdot\overline{\mathbf{w}} - \dfrac{C_0\alpha_0\mathrm{u}_0}{x_0}\,\overline{M}\,\overline{\boldsymbol{\alpha}} : \boldsymbol{\epsilon}(\overline{\mathbf{u}})\,, \\ \rho_0\,\overline{\rho_{\mathrm{dyn}}} = \dfrac{\eta_0}{k_{0_0}\omega_0}\dfrac{\overline{\eta}}{\overline{k}}\,. \end{cases}$$

The equations are written with the dimensionless quantities, and all the constants must be equal. Simplifying, we have:

$$\begin{aligned} \mathrm{u}_0 &= \mathrm{w}_0\,, \\ \tau_0 &= \mathrm{p}_0\,, \\ \tau_0 &= \omega_0\,\rho_0\,\mathrm{u}_0\,x_0\,, \\ C_0 u_0 &= \omega_0\,\tau_0\,x_0\,, \\ \rho_0\,\omega_0\,k_{0_0} &= \eta_0\,. \end{aligned}$$

In the materials in considerations, the magnitude of the bulk modulus and the stiffness matrix is GPa or MPa. For the densities, it is in $10^3\mathrm{kg.m}^{-3}$. We hence choose:

$$C_0 = 10^9\mathrm{Pa}\,,$$

$$\rho_0 = 10^3\mathrm{kg}\cdot\mathrm{m}^{-3}\,,$$

and this follows:

$$\tau_0 = \mathrm{p}_0 = 10^6\mathrm{Pa}\,,$$

$$\omega_0 = 10^3\ \mathrm{rad.s}^{-1}\,,$$

$$\mathrm{u}_0 = \mathrm{w}_0 = 1\ \mathrm{m.s}^{-1}\,,$$

$$x_0 = 1\ \mathrm{m}\,,$$

$$\eta_0 = 10^{-3}\ \mathrm{Pa.s}\,,$$

$$k_{0_0} = 10^{-9}\mathrm{m}^2\,.$$

Note that for different materials or different configurations, these results can be different.

2.3 Problem on bounded domain

For a fixed boundary, we can impose four types of boundary conditions:

$$\text{Type 1} \qquad \begin{cases} \boldsymbol{\tau}\cdot\boldsymbol{n} &= f_t\,, \\ \mathbf{w}\cdot\boldsymbol{n} &= f_w\,, \end{cases}$$

$$\text{Type 2} \qquad \begin{cases} \boldsymbol{\tau}\cdot\boldsymbol{n} &= f_t\,, \\ \mathrm{p} &= f_p\,, \end{cases} \tag{2}$$

$$\text{Type 3} \quad \begin{cases} \mathbf{u} &= f_u, \\ \mathrm{p} &= f_p\,, \end{cases}$$

or

$$\text{Type 4} \quad \begin{cases} \mathbf{u} &= f_u\,, \\ \mathbf{w}\cdot\boldsymbol{n} &= f_w\,, \end{cases}$$

f_u, f_w, f_t, f_p being exterior forces, and $\boldsymbol{n}$ the normal vector along Γ pointing outward. The free boundary conditions are a special case of (2),

$$\begin{cases} \boldsymbol{\tau}\cdot\boldsymbol{n} &= 0\,, \\ \mathrm{p} &= 0\,. \end{cases} \quad \text{Free boundary conditions.}$$

In an interaction problem, the condition of transmission between two poroelastic domains $\Omega_{(I)}$ and $\Omega_{(II)}$ on the interface Γ of normal $\boldsymbol{n}$ is:

$$\begin{cases} \mathbf{u}_{(I)} - \mathbf{u}_{(II)} = 0\,, \\ \mathrm{p}_{(I)} - \mathrm{p}_{(II)} = 0\,, \\ (\mathbf{w}_{(I)} - \mathbf{w}_{(II)})\cdot\boldsymbol{n} = 0\,, \\ (\boldsymbol{\tau}_{(I)} - \boldsymbol{\tau}_{(II)})\cdot\boldsymbol{n} = 0\,. \end{cases}$$

2.4 Physical parameters used for the numerical tests

We list in Table 1 the physical parameters of the porous media considered in this report. The media are filled with brine, which is inviscid in the case of shale and sandstone materials.

Physical parameters	Sandstone	Sand 1	Shale	Sand 2
Porosity ϕ (%)	0.2	0.3	0.16	0.3
Fluid Density ρ_f $(kg.L^{-1})$	1.04	1	1.04	1
Solid Density ρ_s $(kg.L^{-1})$	2.5	2.6	2.21	2.7
Viscosity η $(mPa.s)$	0	1	0	1
Permeability κ_0 (μm^2)	60	10	10	10
Tortuosity $\mathfrak{t}$	2	3	2	3
Solid Bulk Modulus $\mathrm{k_s}$ (GPa)	40	35	7.6	36
Fluid Bulk Modulus $\mathrm{k_f}$ (GPa)	2.5	2.2	2.5	2.2
Frame Bulk Modulus $\mathrm{k_{fr}}$ (GPa)	20	0.4	6.6	7
Frame Shear Modulus $\mathrm{G_{fr}}$ (GPa)	12	0.5	3.96	5

Table 1: Summary of the physical parameters of media in consideration in this report. The parameters for sand 1 are obtained from [18][Table 1], those for sandstone and shale from [11][Table 5], for sand 2 from [20][Table 1]. The values given here are the adimensionnal input values in the program.

3 Formulation of HDG

The poroelastic equations are complex and needs a lot of computational power, because of the size of the system. We choose to use HDG method, to get high-order results. The method is based on DG methods, and present the same advantages to be usable on unstructured meshes, with discontinuous function basis. This is also a method on which we can use hp-adaptivity and that is easily parallelizable because the calculations can be done elementwise. The main drawback of DG methods is the large number of degrees of freedom compared to finite element methods, that increases the computational cost. In HDG methods, the unknowns are expressed as functions of the hybrid unknown, only defined on the boundaries of the elements [23]. The hybrid unknown is taken as a Lagrange multiplier. This reduces the number of degrees of freedom [5], see figure 1. In this section, we apply the HDG method to the poroelastic wave equations.

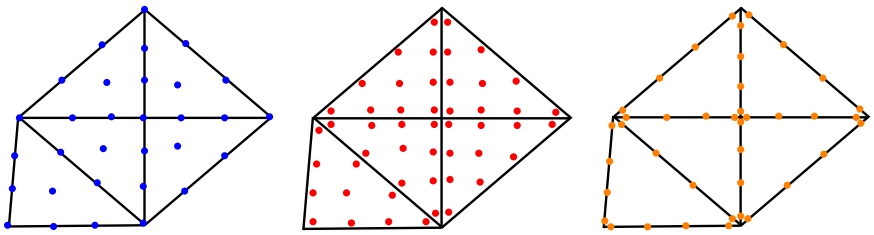

(a) FE (b) DG (c) HDG

Figure 1: Distribution of the degree for finite element method, DG method and HDG method with interpolation degree of order 3.

3.1 Notations

We consider a triangulation $\mathcal{T}_h$ of the domain Ω of dimension d. K denotes an element of the mesh. Here K is a triangle. We denote F a face of the element K, and $\boldsymbol{n}$ the unit normal vector to F.

Given a triangulation $\mathcal{T}_h$, we define the following spaces:

$$
\begin{aligned}
L^2(\Omega) &\text{ the space of square-integrable functions on the domain } \Omega\,,\\
V_p(\Omega) &\text{ the set of polynomials of degree at most } p \text{ on } \Omega\,,\\
\boldsymbol{V}_p(\Omega) &= (V_p(\Omega))^2\,,\\
\boldsymbol{\Sigma}_p(\Omega) &= (V_p(\Omega))^3\,,\\
V_h^p &= \{v \in L^2(\Omega) : v|_K \in V^p(K), \forall K \in \mathcal{T}_h\}\,,\\
\boldsymbol{V}_h^p &= \{\boldsymbol{v} \in (L^2(\Omega))^d : \boldsymbol{v}|_K \in V^p(K), \forall K \in \mathcal{T}_h\}\,,\\
\boldsymbol{\Sigma}_h^p &= \{\boldsymbol{\tau} \in L^2(\Omega)^{d\times d} : \boldsymbol{\tau}|_K \in \boldsymbol{\Sigma}^p(K), \forall K \in \mathcal{T}_h\}\,,\\
M_h &= \{\eta \in L^2(\mathcal{F}_h) : \eta|_F \in V_p(F), \forall K \in \mathcal{F}_h\}\,,\\
\boldsymbol{M}_h &= \{\xi \in (L^2(\mathcal{F}_h))^d : \xi|_F \in (V_p(F))^d, \forall K \in \mathcal{F}_h\}\,.
\end{aligned}
$$

The jumps $[\![\cdot]\!]$ are defined as follows:

- On an interior face $F = \partial K \cap \partial K'$:

$$
[\![\mathbf{w}\cdot\boldsymbol{n}]\!] = \mathbf{w}^K\cdot\boldsymbol{n}^K + \mathbf{w}^{K'}\cdot\boldsymbol{n}^{K'}\,, \qquad [\![\boldsymbol{\tau}\,\boldsymbol{n}]\!] = \boldsymbol{\tau}^K\boldsymbol{n}^K + \boldsymbol{\tau}^{K'}\boldsymbol{n}^{K'}\,, \tag{3}
$$

- On a boundary face:

$$
[\![\mathbf{w}\cdot\boldsymbol{n}]\!] = \mathbf{w}^K\cdot\boldsymbol{n}^K\,, \qquad [\![\boldsymbol{\tau}\,\boldsymbol{n}]\!] = \boldsymbol{\tau}^K\boldsymbol{n}^K\,,
$$

3.2 Local problem

We consider an element K of $\mathcal{T}_h$, and an exact variational solution of (1) on K denoted by $(\mathbf{u}, \mathbf{w}, \boldsymbol{\tau}, \mathrm{p})$. Define the following test functions: $(\tilde{\boldsymbol{u}}, \tilde{\boldsymbol{w}}, \tilde{\boldsymbol{\tau}}, \tilde{\mathrm{p}}) \in (\boldsymbol{V}^p(K)\times\boldsymbol{V}^p(K)\times\boldsymbol{\Sigma}^p(K)\times V^p(K))$. The integration on an element

of (1) gives:

$$\begin{cases} \displaystyle\int_K i\,\omega\,\rho_a\,\mathbf{u}\cdot\tilde{\boldsymbol{u}} + \int_K i\,\omega\,\rho_f\,\mathbf{w}\cdot\tilde{\boldsymbol{u}} - \int_K(\nabla\cdot\boldsymbol{\tau})\cdot\tilde{\boldsymbol{u}} = \int_K \mathbf{f}_u\cdot\tilde{\boldsymbol{u}}\,, \\ \displaystyle\int_K i\,\omega\,\rho_f\,\mathbf{u}\cdot\tilde{\boldsymbol{w}} + \int_K i\,\omega\,\tilde{\rho}\,\mathbf{w}\cdot\tilde{\boldsymbol{w}} + \int_K(\nabla\,\mathrm{p})\cdot\tilde{\boldsymbol{w}} = \int_K \mathbf{f}_w\cdot\tilde{\boldsymbol{w}}\,, \\ \displaystyle\int_K i\,\omega\,\boldsymbol{\tau}:\tilde{\boldsymbol{\tau}} + \int_K i\,\omega\,\boldsymbol{\alpha}\,\mathrm{p}:\tilde{\boldsymbol{\tau}} - \int_K(\mathbf{C}\boldsymbol{\epsilon}(\mathbf{u})):\tilde{\boldsymbol{\tau}} = 0\,, \\ \displaystyle\int_K i\,\omega\,\mathrm{p}\,\tilde{\mathrm{p}} + \int_K M\,\nabla\cdot\mathbf{w}\,\tilde{\mathrm{p}} + \int_K M\,\boldsymbol{\alpha}:\boldsymbol{\epsilon}(\mathbf{u})\,\tilde{\mathrm{p}} = 0\,. \end{cases}$$

By integrating by parts, we have:

$$\begin{cases} \displaystyle\int_K i\,\omega\,\rho_a\,\mathbf{u}\cdot\tilde{\boldsymbol{u}} + \int_K i\,\omega\,\rho_f\,\mathbf{w}\cdot\tilde{\boldsymbol{u}} + \int_K \boldsymbol{\tau}:\nabla\,\tilde{\boldsymbol{u}} - \int_{\partial K}\hat{\boldsymbol{\tau}}_h\boldsymbol{n}\cdot\tilde{\boldsymbol{u}} = \int_K \mathbf{f}_u\cdot\tilde{\boldsymbol{u}}\,, \\ \displaystyle\int_K i\,\omega\,\rho_f\,\mathbf{u}\cdot\tilde{\boldsymbol{w}} + \int_K i\,\omega\,\rho_{\mathrm{dyn}}\,\mathbf{w}\cdot\tilde{\boldsymbol{w}} - \int_K \mathrm{p}\nabla\cdot\tilde{\boldsymbol{w}} + \int_{\partial K}\hat{\mathrm{p}}_h\,\boldsymbol{n}\cdot\tilde{\boldsymbol{w}} = \int_K \mathbf{f}_w\cdot\tilde{\boldsymbol{w}}\,, \\ \displaystyle\int_K i\omega\boldsymbol{\tau}:\tilde{\boldsymbol{\tau}} + \int_K i\omega\boldsymbol{\alpha}\mathrm{p}:\tilde{\boldsymbol{\tau}} + \int_K \mathbf{u}\cdot\nabla\cdot(\mathbf{C}\tilde{\boldsymbol{\tau}}) - \int_{\partial K}\hat{\mathbf{u}}_h\cdot\mathbf{C}\tilde{\boldsymbol{\tau}}\boldsymbol{n} = 0\,, \\ \displaystyle\int_K i\,\omega\,\mathrm{p}\,\tilde{\mathrm{p}} - \int_K M\,\mathbf{w}\cdot\,\nabla\tilde{\mathrm{p}} + \int_{\partial K} M\,(\hat{\mathbf{w}}_h\cdot\boldsymbol{n})\,\tilde{\mathrm{p}} - \int_K M\,(\boldsymbol{\alpha}\mathbf{u})\cdot\nabla\,\tilde{\mathrm{p}} + \int_{\partial K} M\,(\boldsymbol{\alpha}\hat{\mathbf{u}}_h)\cdot\boldsymbol{n}\,\tilde{\mathrm{p}} = 0\,. \end{cases} \tag{4}$$

Remark 2. Note that

$$\int_K(\mathbf{C}\boldsymbol{\epsilon}(\mathbf{u}_h)):\tilde{\boldsymbol{\tau}} = \int_K \boldsymbol{\epsilon}(\mathbf{u}_h):\mathbf{C}\tilde{\boldsymbol{\tau}}$$

because $\mathbf{C}$ is symmetric.

Introduction of the trace variables: The exact solution $(\mathbf{u},\mathbf{w},\boldsymbol{\tau},\mathrm{p})$ on K is approximated by $(\mathbf{u}_h,\,\mathbf{w}_h,\,\boldsymbol{\tau}_h,\,\mathrm{p}_h) \in (\boldsymbol{V}_h^p \times \boldsymbol{V}_h^p \times \boldsymbol{\Sigma}_h^p \times V_h^p)$. The traces on ∂K are approximated by numerical traces $(\hat{\mathbf{u}}_h,\hat{\mathbf{w}}_h,\hat{\boldsymbol{\tau}}_h,\hat{\mathrm{p}}_h)$. We define two unknowns $\boldsymbol{\lambda}_1,\lambda_2$ to replace the numerical traces $\hat{\mathbf{u}}_h$ and $\hat{\mathrm{p}}_h$.

$$\begin{cases} \boldsymbol{\lambda}_1 = \hat{\mathbf{u}}_h, \forall F\in\mathcal{F}_h, \boldsymbol{\lambda}_1\in\boldsymbol{M}_h\,, \\ \lambda_2 = \hat{\mathrm{p}}_h, \forall F\in\mathcal{F}_h, \lambda_2\in M_h\,, \end{cases}$$

The other two traces $(\hat{\boldsymbol{\tau}}_h,\hat{\mathbf{w}}_h)$ are expressed in terms of the numerical traces $\hat{\mathbf{u}}_h$, $\hat{\mathrm{p}}_h$, and the Lagrange multipliers $\boldsymbol{\lambda}_1$, λ_2.

$$\begin{cases} \hat{\boldsymbol{\tau}}_h = \boldsymbol{\tau}_h - \boldsymbol{S}_1(\mathbf{u}_h-\boldsymbol{\lambda}_1)\otimes\boldsymbol{n} - (\mathrm{p}_h-\lambda_2)\boldsymbol{S}_3\,, \\ \hat{\mathbf{w}}_h = \mathbf{w}_h - (\mathrm{p}_h-\lambda_2)\boldsymbol{S}_2\boldsymbol{n} - \boldsymbol{S}_4(\mathbf{u}_h-\boldsymbol{\lambda}_1)\,, \end{cases} \tag{5}$$

where $\boldsymbol{S}_1$, $\boldsymbol{S}_2$, $\boldsymbol{S}_3$, $\boldsymbol{S}_4$ are the stabilization matrices. Note that we use four stabilization parameters while in the works of [15] and [21], they use only two stabilization parameters. This has no influence on the computational

cost of the method. The numerical traces are replaced in (4) to give:

$$\begin{cases} \displaystyle\int_K i\,\omega\,\rho_a\,\mathbf{u}_h\cdot\tilde{\boldsymbol{u}} & \displaystyle+\int_K i\,\omega\,\rho_f\,\mathbf{w}_h\cdot\tilde{\boldsymbol{u}}-\int_K(\nabla\cdot\boldsymbol{\tau}_h)\cdot\tilde{\boldsymbol{u}} \\ & \displaystyle+\int_{\partial K}\boldsymbol{S}_1\,(\mathbf{u}-\boldsymbol{\lambda}_1)\cdot\tilde{\boldsymbol{u}}+\int_{\partial K}(\mathrm{p}_h-\lambda_2)\,(\boldsymbol{S}_3\cdot\boldsymbol{n})\cdot\tilde{\boldsymbol{u}}=\int_K\mathbf{f}_u\cdot\tilde{\boldsymbol{u}}\,, \\ \displaystyle\int_K i\omega\,\rho_f\,\mathbf{u}_h\cdot\tilde{\boldsymbol{w}} & \displaystyle+\int_K i\omega\,\rho_{\mathrm{dyn}}\,\mathbf{w}_h\cdot\tilde{\boldsymbol{w}}-\int_K\mathrm{p}_h\nabla\cdot\tilde{\boldsymbol{w}}+\int_{\partial K}\lambda_2\,\boldsymbol{n}\cdot\tilde{\boldsymbol{w}}=\int_K\mathbf{f}_w\cdot\tilde{\boldsymbol{w}}\,, \\ \displaystyle\int_K i\,\omega\,\boldsymbol{\tau}_h:\tilde{\boldsymbol{\tau}} & \displaystyle+\int_K i\,\omega\,\boldsymbol{\alpha}\mathrm{p}_h:\tilde{\boldsymbol{\tau}}+\int_K\mathbf{u}_h\cdot\nabla\cdot(\mathbf{C}\tilde{\boldsymbol{\tau}})-\int_{\partial K}\boldsymbol{\lambda}_1\cdot\mathbf{C}\,\tilde{\boldsymbol{\tau}}\boldsymbol{n}=0\,, \\ \displaystyle\int_K i\,\omega\,\mathrm{p}_h\,\tilde{\mathrm{p}} & \displaystyle+\int_K M\,\nabla\cdot\mathbf{w}_h\,\tilde{\mathrm{p}}-\int_{\partial K}M\,(\mathrm{p}_h-\lambda_2)\,(\boldsymbol{S}_2\cdot\boldsymbol{n})\cdot\boldsymbol{n}\,\tilde{\mathrm{p}} \\ & \displaystyle-\int_{\partial K}M\,\boldsymbol{S}_4\,(\mathbf{u}_h-\boldsymbol{\lambda}_1)\cdot\boldsymbol{n}\cdot\tilde{\mathrm{p}}-\int_K M\,(\boldsymbol{\alpha}\cdot\mathbf{u}_h)\cdot\nabla\,\tilde{\mathrm{p}}+\int_{\partial K}M\,(\boldsymbol{\alpha}\boldsymbol{\lambda}_1)\cdot\boldsymbol{n}\,\tilde{\mathrm{p}}=0\,. \end{cases}$$

By integrating by parts, we obtain the local problem:

$$\int_K i\,\omega\,\rho_a\,\mathbf{u}_h^K\cdot\tilde{\boldsymbol{u}}+\int_K i\,\omega\,\rho_f\,\mathbf{w}_h^K\cdot\tilde{\boldsymbol{u}}-\int_K(\nabla\cdot\boldsymbol{\tau}_h^K)\cdot\tilde{\boldsymbol{u}}+\int_{\partial K}\boldsymbol{S}_1\,(\mathbf{u}_h^K-\boldsymbol{\lambda}_1)\cdot\tilde{\boldsymbol{u}}$$
$$+\int_{\partial K}(\mathrm{p}_h^K-\lambda_2)\,(\boldsymbol{S}_3\cdot\boldsymbol{n})\cdot\tilde{\boldsymbol{u}}=\int_K\mathbf{f}_u\cdot\tilde{\boldsymbol{u}}\,, \tag{6a}$$

$$\int_K i\,\omega\,\rho_f\,\mathbf{u}_h^K\cdot\tilde{\boldsymbol{w}}+\int_K i\,\omega\,\rho_{\mathrm{dyn}}\,\mathbf{w}_h^K\cdot\tilde{\boldsymbol{w}}-\int_K\mathrm{p}_h^K\nabla\cdot\tilde{\boldsymbol{w}}+\int_{\partial K}\lambda_2\,\boldsymbol{n}\cdot\tilde{\boldsymbol{w}}=\int_K\mathbf{f}_w\cdot\tilde{\boldsymbol{w}}\,, \tag{6b}$$

$$\int_K i\,\omega\,\boldsymbol{\tau}_h^K:\tilde{\boldsymbol{\tau}}+\int_K i\,\omega\,\boldsymbol{\alpha}\,\mathrm{p}_h^K:\tilde{\boldsymbol{\tau}}+\int_K\mathbf{u}_h^K\cdot\nabla\cdot(\mathbf{C}\,\tilde{\boldsymbol{\tau}})-\int_{\partial K}\boldsymbol{\lambda}_1\,\mathbf{C}\,\tilde{\boldsymbol{\tau}}\boldsymbol{n}=0\,, \tag{6c}$$

$$\int_K i\,\omega\,\mathrm{p}_h^K\,\tilde{\mathrm{p}}+\int_K M\nabla\cdot\mathbf{w}_h^K\,\tilde{\mathrm{p}}-\int_{\partial K}M\,(\mathrm{p}_h^K-\lambda_2)\,(\boldsymbol{S}_2\cdot\boldsymbol{n})\cdot\boldsymbol{n}\tilde{\mathrm{p}}-\int_{\partial K}M\,\boldsymbol{S}_4(\mathbf{u}_h^K-\boldsymbol{\lambda}_1)\cdot\boldsymbol{n}\cdot\tilde{\mathrm{p}}$$
$$-\int_K M\,(\boldsymbol{\alpha}\cdot\mathbf{u}_h^K)\cdot\nabla\,\tilde{\mathrm{p}}+\int_{\partial K}M\,(\boldsymbol{\alpha}\boldsymbol{\lambda}_1)\cdot\boldsymbol{n}\,\tilde{\mathrm{p}}=0\,. \tag{6d}$$

3.3 Transmission conditions

The HDG formulation is established by combining the local problem with two transmission conditions at the interfaces of the mesh. Let $(\eta,\,\xi)\in\boldsymbol{M}_h\times M_h$ be two test-functions defined on the faces of the element K, and recall the jumps for an interior face (3), the transmission conditions are:

$$\begin{cases}\displaystyle\sum_{F\in\mathcal{F}_h}\int_F[\![\hat{\boldsymbol{\tau}}_h\,\boldsymbol{n}]\!]\cdot\eta=0\,,\\ \displaystyle\sum_{F\in\mathcal{F}_h}\int_F[\![\hat{\mathbf{w}}_h\cdot\boldsymbol{n}]\!]\,\xi=0\,.\end{cases} \tag{7}$$

Properties Using the expressions of the numerical traces defined in (5), we have:

$$\sum_{F\in\mathcal{F}_h}\int_F[\![\hat{\boldsymbol{\tau}}_h\,\boldsymbol{n}]\!]\cdot\eta=\sum_{K\in\mathcal{T}_h}\int_{\partial K}(\boldsymbol{\tau}_h\,\boldsymbol{n})\cdot\eta-\sum_{K\in\mathcal{T}_h}\int_{\partial K}\boldsymbol{S}_1(\mathbf{u}_h-\hat{\mathbf{u}}_h)\cdot\eta-\sum_{K\in\mathcal{T}_h}\int_{\partial K}(\mathrm{p}_h-\hat{\mathrm{p}}_h)(\boldsymbol{S}_3\,\boldsymbol{n})\cdot\eta\,,$$

and

$$\sum_{F\in\mathcal{F}_h}\int_F[\![\hat{\mathbf{w}}_h\cdot\boldsymbol{n}]\!]\,\xi=\sum_{K\in\mathcal{T}_h}\int_{\partial K}(\mathbf{w}_h\cdot\boldsymbol{n})\,\xi-\sum_{K\in\mathcal{T}_h}\int_{\partial K}(\mathrm{p}_h-\hat{\mathrm{p}}_h)(\boldsymbol{S}_2\,\boldsymbol{n})\cdot\boldsymbol{n}\,\xi-\sum_{K\in\mathcal{T}_h}\int_{\partial K}\boldsymbol{S}_4(\mathbf{u}_h-\hat{\mathbf{u}}_h)\cdot\boldsymbol{n}\,\xi\,.$$

3.4 Boundary conditions

For a face on the boundary, the transmission condition depends on the formulation of the boundary conditions, see section 2.3. Four types of boundary conditions can be imposed on the interface of the domain, using the jumps defined in (3.1):

$$\text{Type 1} \qquad \begin{cases} \displaystyle\int_F [\![\hat{\boldsymbol{\tau}}_h \, \boldsymbol{n}]\!] \cdot \eta = \int_F f_t \cdot \eta \,, \\ \displaystyle\int_F [\![\hat{\mathbf{w}}_h \cdot \boldsymbol{n}]\!] \, \xi = \int_F f_w \, \xi \,, \end{cases} \tag{8}$$

$$\text{Type 2} \qquad \begin{cases} \displaystyle\int_F [\![\hat{\boldsymbol{\tau}}_h \, \boldsymbol{n}]\!] \cdot \eta = \int_F f_t \cdot \eta \,, \\ \mathrm{p}_h = f_p \,, \end{cases}$$

$$\text{Type 3} \qquad \begin{cases} \mathbf{u}_h = f_u, \\ \mathrm{p}_h = f_p \,, \end{cases}$$

or

$$\text{Type 4} \qquad \begin{cases} \mathbf{u}_h = f_u \,, \\ \displaystyle\int_F [\![\hat{\mathbf{w}}_h \cdot \boldsymbol{n}]\!] \, \xi = \int_F f_w \, \xi \,. \end{cases} \tag{9}$$

with f_t, f_w, f_p and f_u exterior forces.

4 Discretization of HDG

The following section details the two-dimensional discretization of the HDG method in the (x, y) plane. From now, we consider the stabilization matrices to be of the form $\boldsymbol{S}_i = \gamma_i \, \mathbf{Id}$ for $i = 1, 4$. In the formulation, the test functions are replaced by φ_i^K and ψ_j^F, the basis functions of V_p. The local solutions are decomposed as:

$$\mathrm{u}_l^K = \sum_{j=1}^{d_i^K} \underline{\mathrm{u}}_{l,j}^K \varphi_j^K \,, \quad \mathrm{w}_l^K = \sum_{j=1}^{d_i^K} \underline{\mathrm{w}}_{l,j}^K \varphi_j^K \,, \quad \tau_{kl}^K = \sum_{j=1}^{d_i^K} \underline{\tau}_{kl,j}^K \varphi_j^K \,, \quad \mathrm{p}^K = \sum_{j=1}^{d_i^K} \underline{\mathrm{p}}^K \varphi_j^K \,, \tag{10}$$

where d_i^K denotes number of degrees of freedom of an element, and with $l = x, y$ and $k = x, y$. The local Lagrange unknowns are decomposed as follows:

$$\lambda_{1l}^F = \sum_{j=1}^{d_i^F} \underline{\lambda_{1l}}_j^F \psi_j^F \,, \qquad \lambda_2^F = \sum_{j=1}^{d_i^F} \underline{\lambda_2}_j^F \psi_j^F \,, \qquad \text{with } l = x, y \,. \tag{11}$$

Define the following elementary matrices:

$$\begin{aligned}
&\mathbb{M}_{ij}^K = \int_K \varphi_i^K \varphi_j^K dX \,, && \mathbb{D}_{vij}^K = \int_K \varphi_j^K \frac{\partial \varphi_i^K}{\partial v} dX \,, && \\
&\mathbb{E}_{ij}^F = \int_F \varphi_i^K \varphi_j^K dS \,, && \mathbb{J}_{vij}^F = \int_F \varphi_i^K \varphi_j^K n_v \, dS \,, && \mathbb{N}_{vij}^F = \int_F \varphi_i^K \varphi_j^K n_v^2 \, dS \,, \\
&\mathbb{F}_{ij}^F = \int_F \psi_j^{\beta(K,l)} \varphi_i^K dS \,, && \mathbb{Q}_{vij}^F = \int_F \psi_j^{\beta(K,l)} \varphi_i^K n_v \, dS \,, && \mathbb{L}_{uvij}^F = \int_F \varphi_i^K \psi_j^{\beta(K,l)} n_u \, n_v \, dS \,, \\
&\mathbb{G}_{ij}^F = \int_F \psi_i^{\beta(K,l)} \psi_j^{\beta(K,l)} dS \,, && \mathbb{H}_{vij}^F = \int_F \psi_i^{\beta(K,l)} \psi_j^{\beta(K,l)} n_v \, dS \,, && \mathbb{O}_{uvij}^F = \int_F \psi_i^{\beta(K,l)} \psi_j^{\beta(K,l)} n_u \, n_v \, dS \,,
\end{aligned} \tag{12}$$

where $\beta(K, l)$ is the global index of the l-th face of the element K and with $u = x, y$, and $v = x, y$.

4.1 Local problem

Because of the size of the system of equations, we present the discretization of each equation of the local problem (6) one by one. For each equation, the local unknowns are decomposed, then the equation is written using the matrices defined in (12).

Discretization of the equation of motion (6a):

$$\begin{cases} \displaystyle\int_K \mathrm{i}\,\omega\,\rho_a^K\,\mathrm{u}_x^K\,\varphi_i^K + \int_K \mathrm{i}\,\omega\,\rho_f^K\,\mathrm{w}_x^K\,\varphi_i^K - \int_K \frac{\partial \tau_{xx}^K}{\partial x}\,\varphi_i^K - \int_K \frac{\partial \tau_{xy}^K}{\partial y}\,\varphi_i^K \\ \displaystyle + \int_{\partial K} \gamma_1^K\,\mathrm{u}_x^K\,\varphi_i^K - \int_{\partial K} \gamma_1^K\,\lambda_{1x}\varphi_i^K + \int_{\partial K} \gamma_3^K\,\mathrm{p}_h^K\,n_x\,\varphi_i^K - \int_{\partial K} \gamma_3^K\,\lambda_2\,n_x\,\varphi_i^K = \int_K f_{ux}\,\varphi_i^K\,, \\ \displaystyle\int_K \mathrm{i}\,\omega\,\rho_a^K\,\mathrm{u}_y^K\,\varphi_i^K + \int_K \mathrm{i}\,\omega\,\rho_f^K\,\mathrm{w}_y^K\,\varphi_i^K - \int_K \frac{\partial \tau_{xy}^K}{\partial x}\,\varphi_i^K - \int_K \frac{\partial \tau_{yy}^K}{\partial y}\,\varphi_i^K \\ \displaystyle + \int_{\partial K} \gamma_1^K\,\mathrm{u}_y^K\,\varphi_i^K - \int_{\partial K} \gamma_1^K\,\lambda_{1y}\varphi_i^K + \int_{\partial K} \gamma_3^K\,\mathrm{p}_h^K\,n_y\,\varphi_i^K - \int_{\partial K} \gamma_3^K\,\lambda_2\,n_y\,\varphi_i^K = \int_K f_{uy}\,\varphi_i^K\,, \end{cases}$$

$$\begin{cases} \mathrm{i}\,\omega\,\rho_a^K\,\mathbb{M}^K\underline{\mathrm{u}}_x^K + \mathrm{i}\,\omega\,\rho_f^K\,\mathbb{M}^K\underline{\mathrm{w}}_x^K - \mathbb{D}_x^{KT}\,\underline{\tau}_{xx}^K - \mathbb{D}_y^{KT}\,\underline{\tau}_{xy}^K + \displaystyle\sum_{l=1}^{3}\gamma_1^{(K,l)}\,\mathbb{E}_l^K\,\underline{\mathrm{u}}_x^K - \sum_{l=1}^{3}\gamma_1^{(K,l)}\,\mathbb{F}_l^K\,\underline{\lambda}_{1x}^{\beta(K,l)} \\ \qquad\qquad + \displaystyle\sum_{l=1}^{3}\gamma_3^{(K,l)}\,\mathbb{J}_{xl}^K\,\underline{\mathrm{p}}^K - \sum_{l=1}^{3}\gamma_3^{(K,l)}\,\mathbb{Q}_{xl}^K\,\underline{\lambda}_2^{\beta(K,l)} = \displaystyle\int_K f_{ux}\,\varphi_i^K\,, \\ \mathrm{i}\omega\,\rho_a^K\,\mathbb{M}^K\underline{\mathrm{u}}_y^K + \mathrm{i}\omega\,\rho_f^K\,\mathbb{M}^K\underline{\mathrm{w}}_y^K - \mathbb{D}_x^{KT}\,\underline{\tau}_{xy}^K - \mathbb{D}_y^{KT}\,\underline{\tau}_{yy}^K + \displaystyle\sum_{l=1}^{3}\gamma_1^{(K,l)}\,\mathbb{E}_l^K\,\underline{\mathrm{u}}_y^K - \sum_{l=1}^{3}\gamma_1^{(K,l)}\,\mathbb{F}_l^K\,\underline{\lambda}_{1y}^{\beta(K,l)} \\ \qquad\qquad + \displaystyle\sum_{l=1}^{3}\gamma_3^{(K,l)}\,\mathbb{J}_{yl}^K\,\underline{\mathrm{p}}^K - \sum_{l=1}^{3}\gamma_3^{(K,l)}\,\mathbb{Q}_{yl}^K\,\underline{\lambda}_2^{\beta(K,l)} = \displaystyle\int_K f_{uy}\,\varphi_i^K\,. \end{cases}$$

Discretization of the second equation of motion (6b):

$$\begin{cases} \displaystyle\int_K \mathrm{i}\,\omega\,\rho_f^K\,\mathrm{u}_x^K\varphi_i^K + \int_K \mathrm{i}\omega\,\tilde{\rho}^K\,\mathrm{w}_x^K\varphi_i^K - \int_K \mathrm{p}_h^K\frac{\partial\varphi_i^K}{\partial x} + \int_{\partial K}\lambda_2\,n_x\,\varphi_i^K = \int_K f_{wx}\,\varphi_i^K\,, \\ \displaystyle\int_K \mathrm{i}\omega\,\rho_f^K\,\mathrm{u}_y^K\varphi_i^K + \int_K \mathrm{i}\omega\,\rho_{\mathrm{dyn}}^K\,\mathrm{w}_y^K\varphi_i^K - \int_K \mathrm{p}_h^K\frac{\partial\varphi_i^K}{\partial y} + \int_{\partial K}\lambda_2\,n_y\,\varphi_i^K = \int_K f_{wy}\,\varphi_i^K\,, \end{cases}$$

$$\begin{cases} \mathrm{i}\omega\,\rho_f^K\,\mathbb{M}^K\underline{\mathrm{u}}_x^K + \mathrm{i}\omega\,\rho_{\mathrm{dyn}}^K\,\mathbb{M}^K\underline{\mathrm{w}}_x^K - \mathbb{D}_x^K,\underline{\mathrm{p}}^K - \displaystyle\sum_{l=1}^{3}\mathbb{Q}_{xl}^K\,\underline{\lambda}_2^{\beta(K,l)} = \int_K f_{wx}\,\varphi_i^K\,, \\ \mathrm{i}\omega\,\rho_f^K\,\mathbb{M}^K\,\underline{\mathrm{u}}_y^K + \mathrm{i}\omega\rho_{\mathrm{dyn}}^K\,\mathbb{M}^K\,\underline{\mathrm{w}}_y^K - \mathbb{D}_y^K\,\underline{\mathrm{p}}^K - \displaystyle\sum_{l=1}^{3}\mathbb{Q}_{yl}^K\,\underline{\lambda}_2^{\beta(K,l)} = \int_K f_{wy}\,\varphi_i^K\,. \end{cases}$$

Discretization of the first constitutive law (6c):

$$
\begin{cases}
\displaystyle\int_K \mathrm{i}\,\omega\,\tau_{xx}^K\,\varphi_i^K \;+\int_K \mathrm{i}\,\omega\,\alpha_{11}\,\mathrm{p}_h^K\,\varphi_i^K \;+\int_K C_{11}\,\mathrm{u}_x^K\,\frac{\partial\varphi_i^K}{\partial x} \;+\int_K C_{13}\,\mathrm{u}_x^K\,\frac{\partial\varphi_i^K}{\partial y} \;+\int_K C_{13}\,\mathrm{u}_y^K\,\frac{\partial\varphi_i^K}{\partial x}\\
\displaystyle+\int_K C_{12}\,\mathrm{u}_y^K\,\frac{\partial\varphi_i^K}{\partial y} \;-\int_{\partial K}\lambda_{1x}\,(C_{11}\varphi_i^K n_x+\,C_{13}\varphi_i^K n_y) \;-\int_{\partial K}\lambda_{1y}\,(C_{13}\varphi_i^K n_x+\,C_{12}\varphi_i^K n_y) = \,0,\\
\displaystyle\int_K \mathrm{i}\,\omega\,\tau_{yy}^K\,\varphi_i^K \;+\int_K \mathrm{i}\,\omega\,\alpha_{22}\,\mathrm{p}_h^K\,\varphi_i^K \;+\int_K C_{12}\,\mathrm{u}_x^K\,\frac{\partial\varphi_i^K}{\partial x} \;+\int_K C_{23}\,\mathrm{u}_x^K\,\frac{\partial\varphi_i^K}{\partial y} \;+\int_K C_{23}\,\mathrm{u}_y^K\,\frac{\partial\varphi_i^K}{\partial x}\\
\displaystyle+\int_K C_{22}\,\mathrm{u}_y^K\,\frac{\partial\varphi_i^K}{\partial y} \;-\int_{\partial K}\lambda_{1x}\,(C_{12}\varphi_i^K n_x+\,C_{23}\varphi_i^K n_y) \;-\int_{\partial K}\lambda_{1y}\,(C_{23}\varphi_i^K n_x+\,C_{22}\varphi_i^K n_y) = \,0,\\
\displaystyle\int_K \mathrm{i}\,\omega\,\tau_{xy}^K\,\varphi_i^K \;+\int_K \mathrm{i}\,\omega\,\alpha_{12}\,\mathrm{p}_h^K\,\varphi_i^K \;+\int_K C_{13}\,\mathrm{u}_x^K\,\frac{\partial\varphi_i^K}{\partial x} \;+\int_K C_{33}\,\mathrm{u}_x^K\,\frac{\partial\varphi_i^K}{\partial y} \;+\int_K C_{33}\,\mathrm{u}_y^K\,\frac{\partial\varphi_i^K}{\partial x}\\
\displaystyle+\int_K C_{23}\,\mathrm{u}_y^K\,\frac{\partial\varphi_i^K}{\partial y} \;-\int_{\partial K}\lambda_{1x}\,(C_{13}\varphi_i^K n_x+\,C_{33}\varphi_i^K n_y) \;-\int_{\partial K}\lambda_{1y}\,(C_{33}\varphi_i^K n_x+\,C_{23}\varphi_i^K n_y) = \,0.
\end{cases}
$$

$$
\begin{cases}
\mathrm{i}\,\omega\,\mathbb{M}^K\,\underline{\tau}_{xx}^K \;+\,\mathrm{i}\,\omega\alpha_{11}\mathbb{M}^K\underline{\mathrm{p}}^K \;+C_{11}\mathbb{D}_x^K\,\underline{\mathrm{u}}_x^K \;+C_{13}\mathbb{D}_y^K\,\underline{\mathrm{u}}_x^K \;+C_{13}\mathbb{D}_x^K\,\underline{\mathrm{u}}_y^K \;+C_{12}\mathbb{D}_y^K\,\underline{\mathrm{u}}_y^K\\
\displaystyle-\sum_{l=1}^{3}\underline{\lambda}_{1x}^{\beta(K,l)}\,(C_{11}\mathbb{Q}_{xl}^K+\,C_{13}\mathbb{Q}_{yl}^K) - \sum_{l=1}^{3}\underline{\lambda}_{1y}^{\beta(K,l)}\,(C_{13}\mathbb{Q}_{xl}^K+\,C_{12}\mathbb{Q}_{yl}^K) = \,0\,,\\
\mathrm{i}\,\omega\,\mathbb{M}^K\,\underline{\tau}_{yy}^K \;+\,\mathrm{i}\,\omega\,\alpha_{22}\,\mathbb{M}^K\,\underline{\mathrm{p}}^K \;+C_{12}\mathbb{D}_x^K\,\underline{\mathrm{u}}_x^K \;+C_{23}\mathbb{D}_y^K\,\underline{\mathrm{u}}_x^K \;+C_{23}\mathbb{D}_x^K\,\underline{\mathrm{u}}_y^K \;+C_{22}\mathbb{D}_y^K\,\underline{\mathrm{u}}_y^K\\
\displaystyle-\sum_{l=1}^{3}\underline{\lambda}_{1x}^{\beta(K,l)}\,(C_{12}\mathbb{Q}_{xl}^K+\,C_{23}\mathbb{Q}_{yl}^K) \;-\sum_{l=1}^{3}\underline{\lambda}_{1y}^{\beta(K,l)}\,(C_{23}\mathbb{Q}_{xl}^K+\,C_{22}\mathbb{Q}_{yl}^K) = \,0\,,\\
\mathrm{i}\,\omega\,\mathbb{M}^K\,\underline{\tau}_{xy}^K \;+\,\mathrm{i}\,\omega\,\alpha_{12}\,\mathbb{M}^K\,\underline{\mathrm{p}}^K \;+C_{13}\mathbb{D}_x^K\,\underline{\mathrm{u}}_x^K \;+C_{33}\mathbb{D}_y^K\,\underline{\mathrm{u}}_x^K \;+C_{33}\mathbb{D}_x^K\,\underline{\mathrm{u}}_y^K \;+C_{23}\mathbb{D}_y^K\,\underline{\mathrm{u}}_y^K\\
\displaystyle-\sum_{l=1}^{3}\underline{\lambda}_{1x}^{\beta(K,l)}\,(C_{13}\mathbb{Q}_{xl}^K+\,C_{33}\mathbb{Q}_{yl}^K) \;-\sum_{l=1}^{3}\underline{\lambda}_{1y}^{\beta(K,l)}\,(C_{33}\mathbb{Q}_{xl}^K+\,C_{23}\mathbb{Q}_{yl}^K) = \,0\,,
\end{cases}
$$

Discretization of the second constitutive law (6d):

$$
\begin{aligned}
&\int_K \mathrm{i}\,\omega\,\mathrm{p}_h^K\,\varphi_i^K \;+\int_K M\,\frac{\partial \mathrm{w}_x^K}{\partial x}\,\varphi_i^K \;+\int_K M\,\frac{\partial \mathrm{w}_y^K}{\partial y}\,\varphi_i^K \;-\int_{\partial K} M\,\mathrm{p}_h^K\,\gamma_2\,(n_x^2\varphi_i^K+\,n_y^2\varphi_i^K)\\
&\qquad+\int_{\partial K} M\,\lambda_2\,\gamma_2\,(n_x^2\varphi_i^K+\,n_y^2\varphi_i^K) \;-\int_{\partial K} M\,\gamma_4\mathrm{u}_x^K\cdot n_x\,\varphi_i^K \;-\int_{\partial K} M\,\gamma_4\mathrm{u}_y^K\cdot n_y\,\varphi_i^K\\
&\qquad+\int_{\partial K} M\,\gamma_4\,\lambda_{1x}\cdot n_x\,\varphi_i^K \;+\int_{\partial K} M\,\gamma_4\,\lambda_{1y}\cdot n_y\varphi_i^K \;-\int_K M\,(\alpha_{11}\mathrm{u}_x^K+\,\alpha_{12}\mathrm{u}_y^K)\frac{\partial\varphi_i^K}{\partial x}\\
&\qquad-\int_K M\,(\alpha_{12}\mathrm{u}_x^K+\,\alpha_{22}\mathrm{u}_y^K)\frac{\partial\varphi_i^K}{\partial y} \;+\int_K M\,(\alpha_{11}\lambda_{1x}+\,\alpha_{12}\lambda_{1y})n_x\,\varphi_i^K\\
&\qquad+\int_K M\,(\alpha_{12}\lambda_{1x}+\,\alpha_{22}\lambda_{1y})n_y\,\varphi_i^K = \,0\,.
\end{aligned}
$$

$$
\begin{aligned}
&\mathrm{i}\,\omega\,\mathbb{M}^K\,\underline{\mathrm{p}}^K + M\mathbb{D}_x^{K^T}\,\underline{\mathrm{w}}_x^K + M\mathbb{D}_y^{K^T}\,\underline{\mathrm{w}}_y^K - \sum_{l=1}^{3} M\,\gamma_2^{(K,l)}\,(\mathbb{N}_{xl}^K\underline{\mathrm{p}}^K + \mathbb{N}_{yl}^K\underline{\mathrm{p}}^K) + \sum_{l=1}^{3} M\,\gamma_2^{(K,l)}\,\underline{\lambda}_2^{\beta(K,l)}(\mathbb{L}_{xxl}^K + \mathbb{L}_{yyl}^K)\\
&\quad - \sum_{l=1}^{3} M\,\gamma_4^{(K,l)}(\mathbb{J}_{xl}^K\,\underline{\mathrm{u}}_x^K + \mathbb{J}_{yl}^K\,\underline{\mathrm{u}}_y^K) + \sum_{l=1}^{3} M\,\gamma_4^{(K,l)}(\mathbb{Q}_{xl}^K\,\underline{\lambda}_{1x}^{\beta(K,l)} + \mathbb{Q}_{yl}^K\underline{\lambda}_{1y}^{\beta(K,l)})\\
&\quad - M\,\alpha_{11}\,\mathbb{D}_x^K\,\mathrm{u}_x^K - M\,\alpha_{12}\mathbb{D}_y^K\,\mathrm{u}_y^K + \sum_{l=1}^{3} M(\alpha_{11}\underline{\lambda}_{1x}^{\beta(K,l)} + \alpha_{12}\underline{\lambda}_{1y}^{\beta(K,l)})\mathbb{Q}_{xl}^K\\
&\quad - M\,\alpha_{12}\,\mathbb{D}_y^K\,\mathrm{u}_x^K - M\,\alpha_{22}\,\mathbb{D}_x^K\,\mathrm{u}_y^K + \sum_{l=1}^{3} M(\alpha_{12}\underline{\lambda}_{1x}^{\beta(K,l)} + \alpha_{22}\,\underline{\lambda}_{1y}^{\beta(K,l)})\,\mathbb{Q}_{yl}^K = 0\,.
\end{aligned}
$$

System : We define the unknowns vectors as:

$$\underline{W}^K = (\underline{\mathrm{u}}_x^K,\, \underline{\mathrm{u}}_y^K,\, \underline{\mathrm{w}}_x^K,\, \underline{\mathrm{w}}_y^K,\, \underline{\tau}_{xx}^K,\, \underline{\tau}_{yy}^K,\, \underline{\tau}_{xy}^K,\, \underline{\mathrm{p}}^K)\,,$$

and

$$\underline{\Lambda}^K = (\underline{\lambda}_{1x}^{\beta(K,1)}, \underline{\lambda}_{1x}^{\beta(K,2)}, \underline{\lambda}_{1x}^{\beta(K,3)}, \underline{\lambda}_{1y}^{\beta(K,1)} \underline{\lambda}_{1y}^{\beta(K,2)}, \underline{\lambda}_{1y}^{\beta(K,3)}, \underline{\lambda}_{2}^{\beta(K,1)}, \underline{\lambda}_{2}^{\beta(K,2)}, \underline{\lambda}_{2}^{\beta(K,3)})\,.$$

The local system obtained from the discretization of (6) can be written as:

$$\mathbb{A}^K\underline{W}^K + \mathbb{B}^K\underline{\Lambda}^K = \mathbb{C}_{\text{source}}^K\,,$$

$\mathbb{C}_{\text{source}}^K$ being the matrix of the external forces, and with:

$$\mathbb{A}^K = \begin{pmatrix} \mathbb{A}_1^K & \mathbb{A}_2^K & \mathbb{A}_3^K & \mathbb{A}_4^K & \mathbb{A}_5^K & \mathbb{A}_6^K & \mathbb{A}_7^K & \mathbb{A}_8^K \end{pmatrix}\,,$$

where

$$\mathbb{A}_1^K = \begin{pmatrix} \mathrm{i}\,\omega\rho_a^K\mathbb{M}^K + \sum_{l=1}^{3}\gamma_1^{(K,l)}\left(\mathbb{N}_{xl}^K + \mathbb{N}_{yl}^K\right) \\ 0 \\ \mathrm{i}\,\omega\rho_f^K\mathbb{M}^K \\ 0 \\ \left(C_{11}\mathbb{D}_x^K + C_{13}\mathbb{D}_y^K\right) \\ \left(C_{12}\mathbb{D}_x^K + C_{23}\mathbb{D}_y^K\right) \\ \left(C_{13}\mathbb{D}_x^K + C_{33}\mathbb{D}_y^K\right) \\ -M\left(\sum_{l=1}^{3}\gamma_4^{(K,l)}\mathbb{J}_{xl}^K + \alpha_{11}\mathbb{D}_x^K + \alpha_{12}\mathbb{D}_y^K\right) \end{pmatrix}, \quad \mathbb{A}_2^K = \begin{pmatrix} 0 \\ \mathrm{i}\,\omega\rho_a^K\mathbb{M}^K + \sum_{l=1}^{3}\gamma_1^{(K,l)}\left(\mathbb{N}_{xl}^K + \mathbb{N}_{yl}^K\right) \\ 0 \\ \mathrm{i}\,\omega\rho_f^K\mathbb{M}^K \\ \left(C_{13}\mathbb{D}_x^K + C_{12}\mathbb{D}_y^K\right) \\ \left(C_{23}\mathbb{D}_x^K + C_{22}\mathbb{D}_y^K\right) \\ \left(C_{33}\mathbb{D}_x^K + C_{23}\mathbb{D}_y^K\right) \\ -M\left(\sum_{l=1}^{3}\gamma_4^{(K,l)}\mathbb{J}_{yl}^K + \alpha_{12}\mathbb{D}_x^K + \alpha_{22}\mathbb{D}_y^K\right) \end{pmatrix},$$

$$\mathbb{A}_3^K = \begin{pmatrix} \mathrm{i}\,\omega\rho_f^K\mathbb{M}^K \\ 0 \\ \mathrm{i}\,\omega\rho_{\text{dyn}}^K\mathbb{M}^K \\ 0 \\ 0 \\ 0 \\ 0 \\ M\mathbb{D}_x^{K^T} \end{pmatrix}, \qquad \mathbb{A}_4^K = \begin{pmatrix} 0 \\ \mathrm{i}\,\omega\rho_f^K\mathbb{M}^K \\ 0 \\ \mathrm{i}\,\omega\rho_{\text{dyn}}^K\mathbb{M}^K \\ 0 \\ 0 \\ 0 \\ M\mathbb{D}_y^{K^T} \end{pmatrix},$$

$$\mathbb{A}_5^K = \begin{pmatrix} -\mathbb{D}_x^{K^T} \\ 0 \\ 0 \\ 0 \\ \mathrm{i}\,\omega\mathbb{M}^K \\ 0 \\ 0 \\ 0 \end{pmatrix}, \qquad \mathbb{A}_6^K = \begin{pmatrix} 0 \\ -\mathbb{D}_y^{K^T} \\ 0 \\ 0 \\ 0 \\ \mathrm{i}\,\omega\mathbb{M}^K \\ 0 \\ 0 \end{pmatrix}, \qquad \mathbb{A}_7^K = \begin{pmatrix} -\mathbb{D}_y^{K^T} \\ -\mathbb{D}_x^{K^T} \\ 0 \\ 0 \\ 0 \\ 0 \\ \mathrm{i}\,\omega\mathbb{M}^K \\ 0 \end{pmatrix},$$

$$\mathbb{A}_8^K = \begin{pmatrix} \sum_{l=1}^{3} \gamma_3^{(K,l)} \mathbb{J}_{xl}^K \\ \sum_{l=1}^{3} \gamma_3^{(K,l)} \mathbb{J}_{yl}^K \\ -\mathbb{D}_x^K \\ -\mathbb{D}_y^K \\ \mathrm{i}\,\omega\alpha_{11}^K \mathbb{M}^K \\ \mathrm{i}\,\omega\alpha_{22}^K \mathbb{M}^K \\ \mathrm{i}\,\omega\alpha_{12}^K \mathbb{M}^K \\ \mathrm{i}\,\omega\mathbb{M}^K - \sum_{l=1}^{3} M\gamma_2^{(K,l)} \left(\mathbb{N}_{xl}^K + \mathbb{N}_{yl}^K\right) \end{pmatrix},$$

and

$$\mathbb{B}^K = \begin{pmatrix} B_{\lambda_{1x},1} & B_{\lambda_{1x},2} & B_{\lambda_{1x},3} & B_{\lambda_{1y},1} & B_{\lambda_{1y},2} & B_{\lambda_{1y},3} & B_{\lambda_2,1} & B_{\lambda_2,2} & B_{\lambda_2,3} \end{pmatrix}$$

with

$$B_{\lambda_{1x},f} = \begin{pmatrix} -\gamma_1^{(K,1)} \mathbb{F}_l^K \\ 0 \\ 0 \\ 0 \\ (-C_{11}\mathbb{Q}_{xl}^K - C_{13}\mathbb{Q}_{yl}^K) \\ (-C_{12}\mathbb{Q}_{xl}^K - C_{23}\mathbb{Q}_{yl}^K) \\ (-C_{13}\mathbb{Q}_{xl}^K - C_{33}\mathbb{Q}_{yl}^K) \\ M\left((\gamma_4^{(K,l)} + \alpha_{11})\mathbb{Q}_{xl}^K + \alpha_{12}\mathbb{Q}_{yl}^K\right) \end{pmatrix}, \qquad B_{\lambda_{1x},f} = \begin{pmatrix} 0 \\ -\gamma_1^{(K,1)} \mathbb{F}_f^K \\ 0 \\ 0 \\ (-C_{13}\mathbb{Q}_{xf}^K - C_{12}\mathbb{Q}_{yf}^K) \\ (-C_{23}\mathbb{Q}_{xf}^K - C_{22}\mathbb{Q}_{yf}^K) \\ (-C_{33}\mathbb{Q}_{xf}^K - C_{23}\mathbb{Q}_{yf}^K) \\ M\left((\gamma_4^{(K,l)} + \alpha_{12})\mathbb{Q}_{xf}^K + \alpha_{22}\mathbb{Q}_{yf}^K\right) \end{pmatrix},$$

$$B_{\lambda_2,f} = \begin{pmatrix} -\gamma_3^{(K,1)} \mathbb{Q}_{xf}^K \\ -\gamma_3^{(K,1)} \mathbb{Q}_{yf}^K \\ \mathbb{Q}_{xf}^K \\ \mathbb{Q}_{yf}^K \\ 0 \\ 0 \\ 0 \\ M\gamma_2^{(K,f)} (\mathbb{L}_{xf}^K + \mathbb{L}_{yf}^K) \end{pmatrix}, \quad \text{for } f = 1, 2, 3\,,$$

and

$$\mathbb{C}^K_{\text{source}} = \begin{pmatrix} \displaystyle\int_K f_{vx}\,\varphi_i^K \\ \displaystyle\int_K f_{vy}\,\varphi_i^K \\ \displaystyle\int_K f_{wx}\,\varphi_i^K \\ \displaystyle\int_K f_{wy}\,\varphi_i^K \\ 0 \\ 0 \\ 0 \\ 0 \end{pmatrix}.$$

4.2 Transmission conditions on an interior face

Recall the transmission condition (7) on an interior face $F = \partial K \cap \partial K'$ such as $\beta(K,l) = \beta(K',g)$:

$$\sum_{F\in\mathcal{F}_h} \int_F [\![\hat{\boldsymbol{\tau}}_h\,\boldsymbol{n}]\!]\cdot\eta = 0\,, \tag{13a}$$

$$\sum_{F\in\mathcal{F}_h} \int_F [\![\hat{\mathbf{w}}_h\cdot\boldsymbol{n}]\!]\,\xi = 0\,. \tag{13b}$$

The expression with the jump on F is expressed as follows:

$$\begin{cases} \displaystyle\int_F \boldsymbol{\tau}_h^K\boldsymbol{n}^K\cdot\eta + \int_F \boldsymbol{\tau}_h^{K'}\boldsymbol{n}^{K'}\cdot\eta - \int_F \boldsymbol{S}_1^K(\mathbf{u}_h^K-\boldsymbol{\lambda}_1)\cdot\eta - \int_F \boldsymbol{S}_1^{K'}(\mathbf{u}_h^{K'}-\boldsymbol{\lambda}_1)\cdot\eta \\ \qquad\qquad - \displaystyle\int_F (\mathrm{p}_h^K-\lambda_2)\boldsymbol{S}_3^K\boldsymbol{n}^K\cdot\eta - \int_F (\mathrm{p}_h^{K'}-\lambda_2)\boldsymbol{S}_3^{K'}\boldsymbol{n}^{K'}\cdot\eta = 0, \\ \displaystyle\int_F \mathbf{w}_h^K\cdot\boldsymbol{n}^K\,\xi + \int_F \mathbf{w}_h^{K'}\cdot\boldsymbol{n}^{K'}\,\xi - \int_F (\mathrm{p}_h^K-\lambda_2)(\boldsymbol{S}_2^K\boldsymbol{n}^K)\cdot\boldsymbol{n}^K\,\xi - \int_F (\mathrm{p}_h^{K'}-\lambda_2)(\boldsymbol{S}_2^{K'}\boldsymbol{n}^{K'})\cdot\boldsymbol{n}^{K'}\,\xi \\ \qquad\qquad - \displaystyle\int_F \boldsymbol{S}_4^K(\mathbf{u}_h^K-\boldsymbol{\lambda}_1)\cdot\boldsymbol{n}^K\cdot\xi - \int_F \boldsymbol{S}_4^{K'}(\mathbf{u}_h^{K'}-\boldsymbol{\lambda}_1)\cdot\boldsymbol{n}^{K'}\,\xi = 0. \end{cases}$$

These equations are discretized on (x,y) by decomposing the unknowns using equations (10) and (11), then they are expressed in terms of the elementary matrices defined in (12).

Discretization of the first transmission equation (13a)

$$
\begin{cases}
\displaystyle\int_F \underline{\tau}_{xx}^K\, n_x^K\, \varphi_j^K\, \psi_i^{\beta(K,l)}\, dS + \int_F \underline{\tau}_{xy}^K\, n_y^K\, \varphi_j^K\, \psi_i^{\beta(K,l)}\, dS + \int_F \underline{\tau}_{xx}^{K'}\, n_x^{K'}\, \varphi_j^K\, \psi_i^{\beta(K',l)}\, dS + \int_F \underline{\tau}_{xy}^{K'}\, n_y^{K'}\, \varphi_j^K\, \psi_i^{\beta(K',l)} dS \\
\qquad - \displaystyle\int_F \gamma_1^{(K,l)}\, \varphi_j^K\, \underline{\mathrm{u}}_x^K\, \psi_i^{\beta(K,l)}\, dS + \int_F \gamma_1^{(K,l)}\, \psi_j^{\beta(K,l)}\, \underline{\lambda}_{1x}^K\, \psi_i^{\beta(K,l)}\, dS \\
\qquad - \displaystyle\int_F \gamma_1^{(K',l)}\, \varphi_j^{K'}\, \underline{\mathrm{u}}_x^{K'}\, \psi_i^{\beta(K',l)}\, dS + \int_F \gamma_1^{(K',l)}\, \psi_j^{\beta(K',l)}\, \underline{\lambda}_{1x}^{K'}\, \psi_i^{\beta(K',l)}\, dS \\
\qquad - \displaystyle\int_F \gamma_3^{(K,l)}\, n_x^K\, \underline{\mathrm{p}}^K\, \varphi_j^K\, \psi_i^{\beta(K,l)}\, dS + \int_F \gamma_3^{(K,l)}\, n_x^K\, \underline{\lambda}_2^K\, \psi_j^{\beta(K,l)}\, \psi_i^{\beta(K,l)}\, dS \\
\qquad - \displaystyle\int_F \gamma_3^{(K',l)}\, n_x^{K'}\, \underline{\mathrm{p}}^{K'}\, \varphi_j^{K'}\, \psi_i^{\beta(K',l)}\, dS + \int_F \gamma_3^{(K',l)}\, n_x^{K'}\, \underline{\lambda}_2^{K'}\, \psi_j^{\beta(K',l)} \psi_i^{\beta(K',l)}\, dS = 0, \\
\displaystyle\int_F \underline{\tau}_{xy}^K\, n_x^K\, \varphi_j^K\, \psi_i^{\beta(K,l)}\, dS + \int_F \underline{\tau}_{yy}^K\, n_y^K\, \varphi_j^K\, \psi_i^{\beta(K,l)}\, dS + \int_F \underline{\tau}_{xy}^{K'}\, n_x^{K'}\, \varphi_j^K\, \psi_i^{\beta(K',l)}\, dS + \int_F \underline{\tau}_{yy}^{K'}\, n_y^{K'}\, \varphi_j^K\, \psi_i^{\beta(K',l)}\, dS \\
\qquad - \displaystyle\int_F \gamma_1^{(K,l)}\, \varphi_j^K\, \underline{\mathrm{u}}_y^K\, \psi_i^{\beta(K,l)}\, dS + \int_F \gamma_1^{(K,l)}\, \varphi_j^K\, \underline{\lambda}_{1y}^K\, \psi_i^{\beta(K,l)}\, dS \\
\qquad - \displaystyle\int_F \gamma_1^{(K',l)}\, \varphi_j^{K'}\, \underline{\mathrm{u}}_y^{K'}\, \psi_i^{\beta(K',l)}\, dS + \int_F \gamma_1^{(K',l)}\, \varphi_j^{K'}\, \underline{\lambda}_{1y}^{K'}\, \psi_i^{\beta(K',l)}\, dS \\
\qquad - \displaystyle\int_F \gamma_3^{(K,l)}\, n_y^K\, \underline{\mathrm{p}}^K\, \varphi_j^K\, \psi_i^{\beta(K,l)}\, dS + \int_F \gamma_3^{(K,l)}\, n_y^K\, \underline{\lambda}_2^K\, \psi_j^{\beta(K,l)}\, \psi_i^{\beta(K,l)}\, dS \\
\qquad - \displaystyle\int_F \gamma_3^{(K',l)}\, n_y^{K'}\, \underline{\mathrm{p}}^{K'}\, \varphi_j^{K'}\, \psi_i^{\beta(K',l)}\, dS + \int_F \gamma_3^{(K',l)}\, n_y^{K'}\, \underline{\lambda}_2^{K'}\, \psi_j^{\beta(K',l)}\, \psi_i^{\beta(K',l)}\, dS = 0.
\end{cases}
$$

$$
\begin{cases}
\mathbb{Q}_{xl}^{K^T}\, \underline{\tau}_{xx}^K + \mathbb{Q}_{yl}^{K^T}\, \underline{\tau}_{xy}^K - \gamma_1^{(K,l)}\, \mathbb{F}_l^{K^T}\, \underline{\mathrm{u}}_x^K + \gamma_1^{(K,l)}\, \mathbb{G}^j\, \underline{\lambda}_{1x}^{\beta(K,l)} - \gamma_3^{(K,l)}\, \mathbb{Q}_{xl}^{K^T}\, \underline{\mathrm{p}}^K + \gamma_3^{(K,l)}\, \mathbb{H}_x^j\, \underline{\lambda}_2^{\beta(K,l)} \\
+\mathbb{Q}_{xl}^{K'^T}\, \underline{\tau}_{xx}^K + \mathbb{Q}_{yl}^{K'^T}\, \underline{\tau}_{xy}^K - \gamma_1^{(K',l)}\, \mathbb{F}_l^{K'^T}\, \underline{\mathrm{u}}_x^K + \gamma_1^{(K',l)}\, \mathbb{G}^j\, \underline{\lambda}_{1x}^{\beta(K',l)} - \gamma_3^{(K',l)}\, \mathbb{Q}_{xl}^{K'^T}\, \underline{\mathrm{p}}^K + \gamma_3^{(K',l)}\, \mathbb{H}_x^j\, \underline{\lambda}_2^{\beta(K',l)} = 0, \\
\mathbb{Q}_{xl}^{K^T}\, \underline{\tau}_{xy}^K + \mathbb{Q}_{yl}^{K^T}\, \underline{\tau}_{yy}^K - \gamma_1^{(K,l)}\, \mathbb{F}_l^{K^T}\, \underline{\mathrm{u}}_y^K + \gamma_1^{(K,l)}\, \mathbb{G}^j\, \underline{\lambda}_{1y}^{\beta(K,l)} - \gamma_3^{(K,l)}\, \mathbb{Q}_{yl}^{K^T}\, \underline{\mathrm{p}}^K + \gamma_3^{(K,l)}\, \mathbb{H}_y^j\, \underline{\lambda}_2^{\beta(K,l)} \\
+\mathbb{Q}_{xl}^{K'^T}\, \underline{\tau}_{xy}^K + \mathbb{Q}_{yl}^{K'^T}\, \underline{\tau}_{yy}^K - \gamma_1^{(K',l)}\, \mathbb{F}_l^{K'^T}\, \underline{\mathrm{u}}_y^K + \gamma_1^{(K',l)}\, \mathbb{G}^j\, \underline{\lambda}_{1y}^{\beta(K',l)} - \gamma_3^{(K',l)}\, \mathbb{Q}_{yl}^{K'^T}\, \underline{\mathrm{p}}^K + \gamma_3^{(K',l)}\, \mathbb{H}_y^j\, \underline{\lambda}_2^{\beta(K',l)} = 0.
\end{cases}
\tag{14}
$$

Discretization of the second transmission condition (13b)

$$
\begin{aligned}
&\int_F \underline{\mathrm{w}}_x^K\, \varphi_j^K\, n_x^K\, \psi_i^{\beta(K,l)} + \int_F \underline{\mathrm{w}}_y^K\, \varphi_j^K\, n_y^K\, \psi_i^{\beta(K,l)} + \int_F \underline{\mathrm{w}}_x^{K'}\, \varphi_j^{K'}\, n_x^{K'}\, \psi_i^{\beta(K',l)} + \int_F \underline{\mathrm{w}}_y^{K'}\, \varphi_j^{K'}\, n_y^{K'}\, \psi_i^{\beta(K',l)} \\
&- \int_F \underline{\mathrm{p}}^K\, \varphi_j^K\, \gamma_2^{(K,l)}\, \psi_i^{\beta(K,l)} - \int_F \underline{\mathrm{p}}^{K'}\, \varphi_j^{K'}\, \gamma_2^{(K',l)}\, \psi_i^{\beta(K',l)} + \int_F \underline{\lambda}_2^K\, \psi_j^{\beta(K,l)}\, \gamma_2^{(K,l)}\, \psi_i^{\beta(K,l)} \\
&+ \int_F \underline{\lambda}_2^{K'}\, \psi_j^{\beta(K',l)}\, \gamma_2^{(K',l)}\, \psi_i^{\beta(K',l)} - \int_F \underline{\mathrm{u}}_x^K\, \varphi_j^K\, \gamma_4^{(K,l)}\, n_x^K\, \psi_i^{\beta(K,l)} - \int_F \underline{\mathrm{u}}_y^K\, \varphi_j^K\, \gamma_4^{(K,l)}\, n_y^K\, \psi_i^{\beta(K,l)} \\
&- \int_F \underline{\mathrm{u}}_x^{K'}\, \varphi_j^{K'}\, \gamma_4^{(K',l)}\, n_x^{K'}\, \psi_i^{\beta(K',l)} - \int_F \underline{\mathrm{u}}_y^{K'}\, \varphi_j^{K'}\, \gamma_4^{(K',l)}\, n_y^{K'}\, \psi_i^{\beta(K',l)} + \int_F \underline{\lambda}_{1x}^K\, \psi_j^{\beta(K,l)}\, \gamma_4^{(K,l)}\, n_x^K\, \psi_i^{\beta(K,l)} \\
&+ \int_F \underline{\lambda}_{1y}^K\, \psi_j^{\beta(K,l)}\, \gamma_4^{(K,l)}\, n_y^K\, \psi_i^{\beta(K,l)} + \int_F \underline{\lambda}_{1x}^{K'}\, \psi_j^{\beta(K',l)}\, \gamma_4^{(K',l)}\, n_x^{K'}\, \psi_i^{\beta(K',l)} + \int_F \underline{\lambda}_{1y}^{K'}\, \psi_j^{\beta(K',l)}\, \gamma_4^{(K',l)}\, n_y^{K'}\, \psi_i^{\beta(K',l)} = 0.
\end{aligned}
$$

$$\begin{aligned}
&\mathbb{Q}_{xl}^{K^T}\,\underline{\mathrm{w}}_x^K + \mathbb{Q}_{yl}^{K^T}\,\underline{\mathrm{w}}_y^K + \mathbb{Q}_{xl}^{K'^T}\,\underline{\mathrm{w}}_x^{K'} + \mathbb{Q}_{yl}^{K'^T}\,\underline{\mathrm{w}}_y^{K'} - \mathbb{F}_l^{K^T}\,\underline{\mathrm{p}}^K\,\gamma_2^{(K,l)} - \mathbb{F}_l^{K'^T}\,\underline{\mathrm{p}}^K\,\gamma_2^{(K',l)} + \mathbb{G}_l^j\gamma_2^{(K,l)}\,\underline{\lambda}_2^K \\
&+ \mathbb{G}_l^j\gamma_2^{(K',l)}\,\underline{\lambda}_2^{K'} - \mathbb{Q}_x^{K^T}\,\underline{\mathrm{u}}_x^K\,\gamma_4^{(K,l)} - \mathbb{Q}_y^{K^T}\,\underline{\mathrm{u}}_y^K\,\gamma_4^{(K,l)} - \mathbb{Q}_x^{K'^T}\,\underline{\mathrm{u}}_x^K\,\gamma_4^{(K',l)} - \mathbb{Q}_y^{K'^T}\,\underline{\mathrm{u}}_y^K\,\gamma_4^{(K',l)} \qquad (15)\\
&+ \mathbb{H}_x^j\,\underline{\lambda}_{1x}^K\,\gamma_4^{(K,l)} + \mathbb{H}_y^j\,\underline{\lambda}_{1y}^K\,\gamma_4^{(K,l)} + \mathbb{H}_x^j\,\underline{\lambda}_{1x}^{K'}\,\gamma_4^{(K',l)} + \mathbb{H}_y^j\,\underline{\lambda}_{1y}^{K'}\,\gamma_4^{(K',l)} = 0.
\end{aligned}$$

System : Equations (14) and (15) are written as a system:

$$\mathbb{P}^K\underline{W}^K + \mathbb{T}^K\underline{\Lambda}^K + \mathcal{R}^K = 0\,,$$

where $\mathcal{R}^K$ represents the contributions from the neighboring elements

$$\mathcal{R}^K = \begin{pmatrix} R_x^{K_1} & R_x^{K_2} & R_x^{K_3} & R_y^{K_1} & R_y^{K_2} & R_y^{K_3} & R_w^{K_1} & R_w^{K_2} & R_w^{K_3}\end{pmatrix}^T,$$

$$\begin{aligned}
R_x^{K_i} = &\begin{pmatrix} -\gamma_1^{(K_i,i)}\mathbb{F}_i^{K_i} & 0 & 0 & 0 & \mathbb{Q}_{xi}^{K_i} & 0 & \mathbb{Q}_{yi}^{K_i} & -\gamma_3^{(K_i,i)}\mathbb{Q}_{xi}^{K_i}\end{pmatrix}\underline{W}^{K_i}\\
&+ \gamma_1^{(K_i,i)}\mathbb{G}^{(K_i,i)}\underline{\lambda}_{1x}^{\beta(K_i,i)} + \gamma_3^{(K_i,i)}\mathbb{H}_x^{(K_i,i)}\underline{\lambda}_2^{\beta(K_i,i)},
\end{aligned}$$

$$\begin{aligned}
R_y^{K_i} = &\begin{pmatrix} 0 & -\gamma_1^{(K_i,i)}\mathbb{F}_i^{K_i} & 0 & 0 & 0 & \mathbb{Q}_{yi}^{K_i} & \mathbb{Q}_{xi}^{K_i} & -\gamma_3^{(K_i,i)}\mathbb{Q}_{yi}^{K_i}\end{pmatrix}\underline{W}^{K_i}\\
&+ \gamma_1^{(K_i,i)}\mathbb{G}^{(K_i,i)}\underline{\lambda}_{1y}^{\beta(K_i,i)} + \gamma_3^{(K_i,i)}\mathbb{H}_y^{(K_i,i)}\underline{\lambda}_2^{\beta(K_i,i)},
\end{aligned}$$

$$\begin{aligned}
R_{\mathrm{w}}^{K_i} = &\begin{pmatrix} -\gamma_4^{(K_i,i)}\mathbb{Q}_x^{\beta(K_i,i)} & -\gamma_4^{(K_i,i)}\mathbb{Q}_y^{\beta(K_i,i)} & \mathbb{Q}_{xi}^{K_i} & \mathbb{Q}_{yi}^{K_i} & 0 & 0 & 0 & -\gamma_2^{(K_i,i)}(\mathbb{L}_{xx}^{K_iT} + \mathbb{L}_{yy}^{K_iT})\end{pmatrix}\underline{W}^{K_i}\\
&+ \gamma_4^{(K_i,i)}\mathbb{H}_x^{(K_i,i)}\underline{\lambda}_{1x}^{\beta(K_i,i)} + \gamma_4^{(K_i,i)}\mathbb{H}_y^{(K_i,i)}\underline{\lambda}_{1y}^{\beta(K_i,i)} + \gamma_2^{(K_i,i)}(\mathbb{O}_{xx}^{(K_i,i)} + \mathbb{O}_{yy}^{(K_i,i)})\underline{\lambda}_2^{\beta(K_i,i)}.
\end{aligned}$$

The elementary matrices $\mathbb{P}^K$ and $\mathbb{T}^K$ are:

$$\mathbb{P}^K = \begin{pmatrix}
-\gamma_1^{(K,1)}\mathbb{F}_1^{K^T} & 0 & 0 & 0 & \mathbb{Q}_{x1}^{K^T} & 0 & \mathbb{Q}_{y1}^{K^T} & -\gamma_3^{(K,1)}\mathbb{Q}_{x1}^{K^T}\\
-\gamma_1^{(K,2)}\mathbb{F}_2^{K^T} & 0 & 0 & 0 & \mathbb{Q}_{x2}^{K^T} & 0 & \mathbb{Q}_{y2}^{K^T} & -\gamma_3^{(K,2)}\mathbb{Q}_{x2}K^T\\
-\gamma_1^{(K,3)}\mathbb{F}_3^{K^T} & 0 & 0 & 0 & \mathbb{Q}_{x3}^{K^T} & 0 & \mathbb{Q}_{y3}^{K^T} & -\gamma_3^{(K,3)}\mathbb{Q}_{x3}^{K^T}\\
0 & -\gamma_1^{(K,1)}\mathbb{F}_1^{K^T} & 0 & 0 & 0 & \mathbb{Q}_{y1}^{K^T} & \mathbb{Q}_{x1}^{K^T} & -\gamma_3^{(K,1)}\mathbb{Q}_{y1}^{K^T}\\
0 & -\gamma_1^{(K,2)}\mathbb{F}_2^{K^T} & 0 & 0 & 0 & \mathbb{Q}_{y2}^{K^T} & \mathbb{Q}_{x2}^{K^T} & -\gamma_3^{(K,2)}\mathbb{Q}_{y2}^{K^T}\\
0 & -\gamma_1^{(K,3)}\mathbb{F}_3^{K^T} & 0 & 0 & 0 & \mathbb{Q}_{y3}^{K^T} & \mathbb{Q}_{x3}^{K^T} & -\gamma_3^{(K,3)}\mathbb{Q}_{y3}^{K^T}\\
-\mathbb{Q}_x^{K^T}\gamma_4^{(K,1)} & -\mathbb{Q}_y^{K^T}\gamma_4^{(K,1)} & \mathbb{Q}_{x1}^{K^T} & \mathbb{Q}_{y1}^{K^T} & 0 & 0 & 0 & -\gamma_2^{(K,1)}\mathbb{F}_1^{K^T}\\
-\mathbb{Q}_x^{K^T}\gamma_4^{(K,2)} & -\mathbb{Q}_y^{K^T}\gamma_4^{(K,2)} & \mathbb{Q}_{x2}^{K^T} & \mathbb{Q}_{y2}^{K^T} & 0 & 0 & 0 & -\gamma_2^{(K,2)}\mathbb{F}_2^{K^T}\\
-\mathbb{Q}_x^{K^T}\gamma_4^{(K,3)} & -\mathbb{Q}_y^{K^T}\gamma_4^{(K,3)} & \mathbb{Q}_{x3}^{K^T} & \mathbb{Q}_{y3}^{K^T} & 0 & 0 & 0 & -\gamma_2^{(K,3)}\mathbb{F}_3^{K^T}
\end{pmatrix},$$

$$\mathbb{T}^K = \begin{pmatrix}
\gamma_1^{(K,1)}\mathbb{G}^{\beta(K,1)} & 0 & 0 & 0 & 0 & 0 & \dots\\
0 & \gamma_1^{(K,2)}\mathbb{G}^{\beta(K,2)} & 0 & 0 & 0 & 0 & \dots\\
0 & 0 & \gamma_1^{(K,3)}\mathbb{G}^{\beta(K,3)} & 0 & 0 & 0 & \dots\\
0 & 0 & 0 & \gamma_1^{(K,1)}\mathbb{G}^{\beta(K,1)} & 0 & 0 & \dots\\
0 & 0 & 0 & 0 & \gamma_1^{(K,2)}\mathbb{G}^{\beta(K,2)} & 0 & \dots\\
0 & 0 & 0 & 0 & 0 & \gamma_1^{(K,3)}\mathbb{G}^{\beta(K,3)} & \dots\\
\gamma_4^{(K,1)}\mathbb{H}_x^{\beta(K,1)} & 0 & 0 & \gamma_4^{(K,1)}\mathbb{H}_y^{\beta(K,1)} & 0 & 0 & \dots\\
0 & \gamma_4^{(K,2)}\mathbb{H}_x^{\beta(K,2)} & 0 & 0 & \gamma_4^{(K,2)}\mathbb{H}_y^{\beta(K,2)} & 0 & \dots\\
0 & 0 & \gamma_4(K,3)\mathbb{H}_x^{\beta(K,3)} & 0 & 0 & \gamma_4^{(K,3)}\mathbb{H}_y^{\beta(K,3)} & \dots
\end{pmatrix}$$

$$\begin{pmatrix}
\dots & \gamma_3^{(K,1)}\mathbb{H}_x^{\beta(K,1)} & 0 & 0 & \\
\dots & 0 & \gamma_3^{(K,2)}\mathbb{H}_x^{\beta(K,2)} & 0 & \\
\dots & 0 & 0 & \gamma_3^{(K,3)}\mathbb{H}_x^{\beta(K,3)} & \\
\dots & \gamma_3^{(K,1)}\mathbb{H}_y^{\beta(K,1)} & 0 & 0 & \\
\dots & 0 & 0 & \gamma_3^{(K,2)}\mathbb{H}_y^{\beta(K,2)} & 0 \\
\dots & 0 & 0 & \gamma_3^{(K,3)}\mathbb{H}_y^{\beta(K,3)} & \\
\dots & \gamma_2^{(K,1)}\mathbb{G}_1^{\beta(K,l)} & 0 & 0 & \\
\dots & 0 & \gamma_2^{(K,2)}\mathbb{G}_2^{\beta(K,l)} & 0 & \\
\dots & 0 & 0 & \gamma_2^{(K,3)}\mathbb{G}_3^{\beta(K,l)} &
\end{pmatrix}.$$

4.3 Discretization of the transmission condition for a boundary face

In the case of a face on the edge of the mesh, the transmission condition is modified. The transmission can be expressed as the following system

$$\mathbb{P}^K \underline{W}^K + \mathbb{T}^K \underline{\Lambda}^K + \mathcal{R}^K = \mathbb{S}^K_{\text{inc}},$$

with $\mathbb{S}^K_{\text{inc}}$ representing the exterior forces applied on the element. In section 3.4, we have detailed four conditions that can be imposed on the boundary of the mesh. We can first impose the continuity of $\boldsymbol{\tau}_h \cdot \boldsymbol{n}$ and $\mathbf{w} \cdot \boldsymbol{n}$, see equation (8). In this case, the elementary matrices $\mathbb{P}^K$ and $\mathbb{T}^K$ are not modified. In the following, we detail the expression of the elementary matrices $\mathbb{P}^K$ and $\mathbb{T}^K$ in the case where we impose the continuity of $\mathbf{u}$ and p, as in equation (9). The two other formulations for the boundary conditions are linear combinations of these two formulations. From equation (9), we impose:

$$\begin{cases} \mathbf{u}_h = f_u, \\ \mathrm{p}_h = f_p, \end{cases} \quad \Rightarrow \quad \begin{cases} \underline{\boldsymbol{\lambda}}_1 = f_u, \\ \underline{\lambda}_2 = f_p, \end{cases}$$

with f_u and f_p exterior forces. Let us consider an element K that has the face 1 on the boundary of the domain Ω. In this case, the elementary matrices become:

$$\mathbb{P}^K = \begin{pmatrix}
0 & 0 & 0 & 0 & 0 & 0 & 0 & 0 \\
-\gamma_1^{(K,2)}\mathbb{F}_2^{K^T} & 0 & 0 & 0 & \mathbb{Q}_{x2}^{K^T} & 0 & \mathbb{Q}_{y2}^{K^T} & -\gamma_3^{(K,2)}\mathbb{Q}_{x2}K^T \\
-\gamma_1^{(K,3)}\mathbb{F}_3^{K^T} & 0 & 0 & 0 & \mathbb{Q}_{x3}^{K^T} & 0 & \mathbb{Q}_{y3}^{K^T} & -\gamma_3^{(K,3)}\mathbb{Q}_{x3}^{K^T} \\
0 & 0 & 0 & 0 & 0 & 0 & 0 & 0 \\
0 & -\gamma_1^{(K,2)}\mathbb{F}_2^{K^T} & 0 & 0 & 0 & \mathbb{Q}_{y2}^{K^T} & \mathbb{Q}_{x2}^{K^T} & -\gamma_3^{(K,2)}\mathbb{Q}_{y2}^{K^T} \\
0 & -\gamma_1^{(K,3)}\mathbb{F}_3^{K^T} & 0 & 0 & 0 & \mathbb{Q}_{y3}^{K^T} & \mathbb{Q}_{x3}^{K^T} & -\gamma_3^{(K,3)}\mathbb{Q}_{y3}^{K^T} \\
0 & 0 & 0 & 0 & 0 & 0 & 0 & 0 \\
-\mathbb{Q}_x^{K^T}\gamma_4^{(K,2)} & -\mathbb{Q}_y^{K^T}\gamma_4^{(K,2)} & \mathbb{Q}_{x2}^{K^T} & \mathbb{Q}_{y2}^{K^T} & 0 & 0 & 0 & -\gamma_2^{(K,2)}\mathbb{L}_{x2}^{K^T} - \gamma_2^{(K,2)}\mathbb{L}_{y2}^{K^T} \\
-\mathbb{Q}_x^{K^T}\gamma_4^{(K,3)} & -\mathbb{Q}_y^{K^T}\gamma_4^{(K,3)} & \mathbb{Q}_{x3}^{K^T} & \mathbb{Q}_{y3}^{K^T} & 0 & 0 & 0 & -\gamma_2^{(K,3)}\mathbb{L}_{x3}^{K^T} - \gamma_2^{(K,3)}\mathbb{L}_{y3}^{K^T}
\end{pmatrix},$$

and

$$\mathbb{T}^K = \begin{pmatrix}
\mathbf{Id} & 0 & 0 & 0 & 0 & 0 & \dots \\
0 & \gamma_1^{(K,2)}\mathbb{G}^{\beta(K,2)} & 0 & 0 & 0 & 0 & \dots \\
0 & 0 & \gamma_1^{(K,3)}\mathbb{G}^{\beta(K,3)} & 0 & 0 & 0 & \dots \\
0 & 0 & 0 & \mathbf{Id} & 0 & 0 & \dots \\
0 & 0 & 0 & 0 & \gamma_1^{(K,2)}\mathbb{G}^{\beta(K,2)} & 0 & \dots \\
0 & 0 & 0 & 0 & 0 & \gamma_1^{(K,3)}\mathbb{G}^{\beta(K,3)} & \dots \\
0 & 0 & 0 & 0 & 0 & 0 & \dots \\
0 & \gamma_4^{(K,2)}\mathbb{H}_x^{\beta(K,2)} & 0 & 0 & \gamma_4^{(K,2)}\mathbb{H}_y^{\beta(K,2)} & 0 & \dots \\
0 & 0 & \gamma_4^{(K,3)}\mathbb{H}_x^{\beta(K,3)} & 0 & 0 & \gamma_4^{(K,3)}\mathbb{H}_y^{\beta(K,3)} & \dots
\end{pmatrix}$$

$$\left.\begin{array}{cccc}
... & 0 & 0 & 0 \\
... & 0 & \gamma_3^{(K,2)}\mathbb{H}_x^{\beta(K,2)} & 0 \\
... & 0 & 0 & \gamma_3^{(K,3)}\mathbb{H}_x^{\beta(K,3)} \\
... & 0 & 0 & 0 \\
... & 0 & \gamma_3^{(K,2)}\mathbb{H}_y^{\beta(K,2)} & 0 \\
... & 0 & 0 & \gamma_3^{(K,3)}\mathbb{H}_y^{\beta(K,3)} \\
... & \mathbf{Id} & 0 & 0 \\
... & 0 & \gamma_2^{(K,2)}\mathbb{O}_{xy}^{\beta(K,l)} & 0 \\
... & 0 & 0 & \gamma_2^{(K,3)}\mathbb{O}_{xy}^{\beta(K,l)})
\end{array}\right) .$$

4.4 Resolution using HDG method

For an element K, we have built two local systems:

$$\mathbb{A}\,\underline{W}^K \,+\, \mathbb{B}\,\underline{\Lambda}^K \,=\, \mathbb{C}^K_{\text{source}} \tag{16}$$

and

$$\mathbb{P}^K\,\underline{W}^K \,+\, \mathbb{T}^K\,\underline{\Lambda}^K \,+\, \mathcal{R}^K \,=\, \mathbb{S}^K_{\text{inc}}\,. \tag{17}$$

Let N_{face} be the number of edgess of the mesh. We define the global vector that gathers all the elementary Lagrange vectors:

$$\underline{\Lambda} \,=\, (\underline{\boldsymbol{\lambda}}_1^1,\, \underline{\lambda}_2^1,\, ...,\, \underline{\boldsymbol{\lambda}}_1^{N_{face}},\, \underline{\lambda}_2^{N_{face}})\,.$$

Define also the local trace operator $\mathcal{A}_{HDG}$ that links the local degrees of freedom on an element K to the global degrees of freedom of the Lagrange multiplier $\underline{\Lambda}$. This means, for an element K, that

$$\mathcal{A}^K_{HDG}\,\underline{\Lambda} \,=\, \underline{\Lambda}^K\,.$$

Equation (16) is written as:

$$\mathbb{A}^K\underline{W}^K = \mathbb{C}^K_{\text{source}} - \mathbb{B}^K\mathcal{A}^K_{HDG}\underline{\Lambda}\,.$$

Assuming that the mesh is such that $\mathbb{A}^K$ can be inverted for each element, we have:

$$\underline{W}^K = -(\mathbb{A}^K)^{-1}\mathbb{B}^K\mathcal{A}^K_{HDG}\underline{\Lambda} + (\mathbb{A}^K)^{-1}\mathbb{C}^K_{\text{source}}\,. \tag{18}$$

The transmission condition equation (17) is summed on all the faces of each element:

$$\sum_{K\in\mathcal{T}_h}(\mathcal{A}^K_{HDG})^T\left(\mathbb{P}^K\underline{W}^K + \mathbb{T}^K\mathcal{A}^K_{HDG}\underline{\Lambda}\right) = \mathbb{S}_{\text{inc}}\,.$$

Then $\underline{W}^K$ is replaced by its expression in (18):

$$\sum_{K\in\mathcal{T}_h}(\mathcal{A}^K_{HDG})^T\left(\mathbb{P}^K(\mathbb{A}^K)^{-1}\mathbb{C}^K_{\text{source}} - \mathbb{P}^K(\mathbb{A}^K)^{-1}\mathbb{B}^K\mathcal{A}^K_{HDG}\underline{\Lambda} + \mathbb{T}^K\mathcal{A}^K_{HDG}\underline{\Lambda}\right) = \mathbb{S}_{\text{inc}}\,,$$

which means,

$$\sum_{K\in\mathcal{T}_h}(\mathcal{A}^K_{HDG})^T\left(-\mathbb{P}^K(\mathbb{A}^K)^{-1}\mathbb{B}^K + \mathbb{T}^K\right)\mathcal{A}^K_{HDG}\underline{\Lambda} = -\sum_{K\in\mathcal{T}_h}(\mathcal{A}^K_{HDG})^T\,\mathbb{P}^K(\mathbb{A}^K)^{-1}\,\mathbb{C}^K_{\text{source}} + \mathbb{S}_{\text{inc}}\,.$$

The global problem writes:

$$\mathbb{K}\underline{\Lambda} = \mathbb{S}\,,$$

with $\mathbb{K} = \sum_{K\in\mathcal{T}_h}(\mathcal{A}^K_{HDG})^T\left(-\mathbb{P}^K(\mathbb{A}^K)^{-1}\mathbb{B}^K + \mathbb{T}^K\right)$ and $\mathbb{S} = -\sum_{K\in\mathcal{T}_h}(\mathcal{A}^K_{HDG})^T\,\mathbb{P}^K(\mathbb{A}^K)^{-1}\,\mathbb{C}^K_{\text{source}} + \mathbb{S}_{\text{inc}}$.

The resolution can be divided in four steps, detailed in the following algorithm. First, we build the stiffness matrix $\mathbb{K}$ and the source matrix $\mathbb{S}$. These calculations can be done element by element. Then the global system is resolved and the solution is constructed. We use the MUMPS direct solver for the resolution of the linear system, and this is the only step that is global.

Algorithm 1 Resolution with HDG Method

Step 1: Construction of the stiffness matrix
for $K = 1, N_{elem}$ **do**
Compute the matrices $\mathbb{M}^K$ and $\mathbb{D}_v^K$, with $v = x, y$.
for $l = 1, 3$ (4) **do**
Compute the matrices $\mathbb{E}_l^K$, $\mathbb{F}_l^K$, $\mathbb{G}_l^K$, $\mathbb{Q}_{lv}^K$, $\mathbb{J}_{lv}^K$, $\mathbb{H}_{lv}^K$, $\mathbb{N}_{lv}^K$, $\mathbb{O}_{lv}^K$, $\mathbb{L}_{lv}^K$ with $v = x, y$.
end for
Compute the matrices $\mathbb{A}^K$,$(\mathbb{A}^K)^{-1}$, $\mathbb{B}^K$.
Compute $\mathbb{V}^K = (\mathbb{A}^K)^{-1}\mathbb{B}$.
Compute $\mathbb{P}^K$, and $\mathbb{T}^K$ with BC.
Compute $\mathbb{K}^K = \mathbb{P}^K(\mathbb{A}^K)^{-1}\mathbb{B}^K + \mathbb{T}^K$.
Use the $\mathcal{A}_{HDG}$ operator to know the global degrees of freedom of the element and fill the global matrix $\mathbb{K}$.
end for

Step 2: Construction of the source term
Localisation of the point source
for $K = 1, N_{elem}$ **do**
Compute the local matrices $\mathbb{C}^K_{\text{source}}$ and $\mathbb{S}^K_{\text{inc}}$.
Compute $\mathbb{P}^K(\mathbb{A}^K)^{-1}\mathbb{C}^K_{\text{source}}$.
Use the $\mathcal{A}_{HDG}$ operator to know the global degrees of freedom of the element and fill the global matrix $\mathbb{S}$.
end for

Step 3: Resolution of the global system
Resolution of $\mathbb{K}\underline{\Lambda} = \mathbb{S}$ with MUMPS .

Step 4: Reconstruction of the solution
for $K = 1, N_{elem}$ **do**
Compute the solutions $\underline{W}^K$ using the $\mathcal{A}^K_{HDG}$ operator:
$\underline{W}^K = -(\mathbb{A}^K)^{-1}\mathbb{B}^K\mathcal{A}^K_{HDG}\underline{\Lambda}$.
end for

5 Numerical results

In this section, we first present numerical tests in order to validate the code by comparing with analytical solutions developed in [1]. Secondly, we investigate the order of convergence of the method and the influence of the stabilization parameters.

5.1 Validation of the numerical code for scattering of a plane wave by a penetrable porous medium

We first want to validate the implementation of the method. In this section, we set the stabilization parameters $(\gamma_1, \gamma_2, \gamma_3, \gamma_4)$ to 1. We consider a circular domain composed of two different poroelastic media, see figure 2(a). The interior medium of composed of Sand1 while the second one is composed of Sandstone. The parameters of these media are detailed in Tab. 1. Analytical solutions for this configuration have been developped in section 9 of [1]. The incident plane wave is a compression wave corresponding to the P-wave with the following form:

$$
\begin{aligned}
\mathbf{u}_{\mathrm{P}} &= e^{\mathrm{i}\,\mathbf{k}_{\mathrm{P}}\cdot\boldsymbol{x}}\,(\mathrm{i}\omega)\,\widehat{\mathbf{d}} \quad , \quad \mathbf{w}_{\mathrm{P}} = \beta_{\mathrm{P}}\,e^{\mathrm{i}\,\mathbf{k}_{\mathrm{P}}\cdot\boldsymbol{x}}\,(\mathrm{i}\omega)\,\widehat{\mathbf{d}}\,,\\
\boldsymbol{\tau}_{\mathrm{P}} &= \mathrm{i}\omega\,\mathsf{s}_{\mathrm{P}}(\omega)\,e^{\mathrm{i}\mathbf{k}\cdot\boldsymbol{x}}\left(2\,\mu_{\mathrm{fr}}\,\widehat{\mathbf{d}}\otimes\widehat{\mathbf{d}} + \left(-\tfrac{2}{3}\mu_{\mathrm{fr}} + \mathrm{k}_{\mathrm{fr}} + M\,\alpha^2 + \beta_{\mathrm{P}}\,\alpha\,M\right)\mathbf{Id}\right),\\
\mathrm{p}_{\mathrm{P}} &= \mathrm{i}\omega\,\mathsf{s}_{\mathrm{P}}(\omega)\,(-M\,\beta_{\mathrm{P}} - M\,\alpha)\,e^{\mathrm{i}\mathbf{k}_{\mathrm{P}}\cdot\boldsymbol{x}},
\end{aligned}
$$

with

$$
\begin{cases}
\mathbf{k}_{\mathrm{P}} \;=\; \omega\, \mathsf{s}_{\mathrm{P}}(\omega)\, \widehat{\mathbf{d}} \quad , \quad |\widehat{\mathbf{d}}| = 1 \text{ the polarization} \;, \\
\mathsf{s}_{\mathrm{P}}(\omega) \text{ given by } \mathsf{s}_{\mathrm{P}}^2 \;=\; \dfrac{\operatorname{tr} C}{\det B} - \sqrt{\left(\dfrac{\operatorname{tr} C}{\det B}\right)^2 - 4\dfrac{\det A}{\det B}}\,, \\
\beta_{\mathrm{P}} \;=\; -\dfrac{H\,\mathsf{s}^2(\omega) - \rho_a}{\alpha\, M\, \mathsf{s}_{\mathrm{P}}(\omega) \;- \rho_f}\,, \\
\operatorname{tr} C(\omega) \;=\; \rho_{\mathrm{dyn}}(\omega)\, H \;-\; 2\alpha\, M\, \rho_f \;+\; \rho_a\, M\,, \\
\det B \;\;\;=\; M\, H \;-\; (\alpha\, M)^2 \;=\; M\,(\lambda_{\mathrm{fr}} \;+\; 2\mu_{\mathrm{fr}})\,, \\
\det A(\omega) \;=\; \rho_a\, \rho_{\mathrm{dyn}}(\omega) \;-\; \rho_f^2\,.
\end{cases}
$$

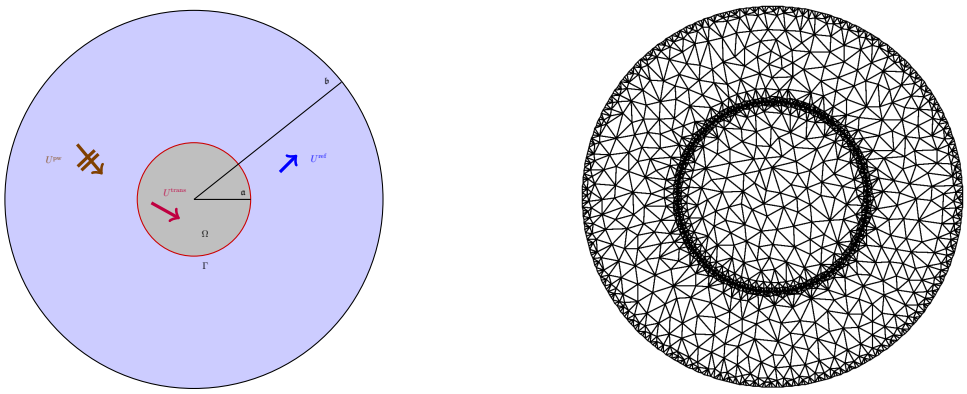

(a) Domain (b) Coarsest mesh

Figure 2: Scattering of a plane wave by a penetrable poroelastic inclusion. The inclusion occupies the domain denoted by Ω. The cross section of the inclusion is a disc of radius denoted by $\mathfrak{a}$. The exterior domain is an annulus between $r = \mathfrak{a}$ and $r = \mathfrak{b}$. In the numerical test, we have $\mathfrak{a} = 5$m and $\mathfrak{b} = 10$m.

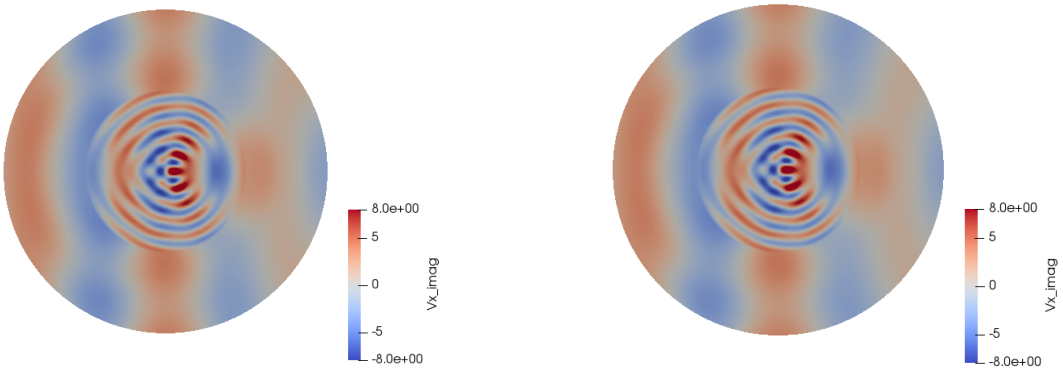

(a) Numerical solution (b) Analytical solution

Figure 3: Numerical and analytical solutions for the scattering of a plane wave by a penetrable poroelastic inclusion at frequency $f = 500$Hz. The result is the imaginary part of the horizontal solid velocity.

Figure 3 shows the analytical and numerical solutions for the test-case with the mesh from figure 2(b) and order 3 of discretization. We display the error between the numerical results and the analytical solutions for mesh 1 for the scattering of a plane wave in Sandstone from a porous inclusion composed of Sand1 in figure 2.

Relative error on V_x (%)	Relative error on V_y (%)	Relative error on W_x (%)	Relative error on W_y (%)	Relative error on S_{xx} (%)	Relative error on S_{yy} (%)	Relative error on S_{xy}(%)	Relative error on P (%)
0.53	0.70	0.53	0.70	0.41	0.44	1.2	1.1

Table 2: Relative errors of the HDG method for the experiment shown in figure 3 For P wave, at frequency $f = 500$Hz with $\theta = 10°$ and boundary conditions of type 1.

5.2 Influence of the stabilization parameters on the error and order of convergence

Next, we want to study the order of convergence of the method in terms of the size of mesh. For that, we use four meshes with straight edges generated by the software Triangle. The coarsest mesh is presented in figure 2(b). Subsequently, finer meshes are obtained from the precedent by the subdivision of every triangles in four new elements. The characteristics of the meshes are summarized in table 3. The size of the mesh corresponds to the longest edge of the elements in the mesh.

	Mesh 1	Mesh 2	Mesh 3	Mesh 4
Size of the mesh (m)	1.514	0.757	0.379	0.189
Number of elements	3270	13080	52320	209280

Table 3: Characteristics of the meshes used for the convergence curves.

We have observed that the accuracy of the method and the order of convergence of the method depends on the presence of the stabilization parameters. Recall that we have defined the stabilization matrices in (5), and we have considered them as diagonal matrices $\boldsymbol{S}_i = \gamma_i \, \mathbf{Id}$ for $i = 1, 4$.

$$\begin{cases} \hat{\boldsymbol{\tau}}_h = \boldsymbol{\tau}_h - \boldsymbol{S}_1(\mathbf{u}_h - \boldsymbol{\lambda}_1) \otimes \boldsymbol{n} - (\mathrm{p}_h - \lambda_2)\boldsymbol{S}_3 \,, \\ \hat{\mathbf{w}}_h = \mathbf{w}_h - (\mathrm{p}_h - \lambda_2)\boldsymbol{S}_2\boldsymbol{n} - \boldsymbol{S}_4(\mathbf{u}_h - \boldsymbol{\lambda}_1) \,, \end{cases} \tag{20}$$

$\boldsymbol{S}_1$ represents the stabilization on the solid frame, $\boldsymbol{S}_2$ on the fluid, while $\boldsymbol{S}_3$ and $\boldsymbol{S}_4$ represent the coupling of these materials that composed the porous medium. In this study, we want to highlight the influencce of each of those stabilization matrices in the HDG method. For several orders of HDG method, we first show the error of the method function of the size of the mesh in figure 4 with every stabilization parameters set to 1. The method seems to converge with order $p+1$. We only display the component of the solid velocity $\mathbf{u}_x$, the other components have the same order of convergence. It is also the case with the four parameters set to the same value (0.1). Note that we do not obtain order $p+2$ because we do not perform post-processing on the solution.

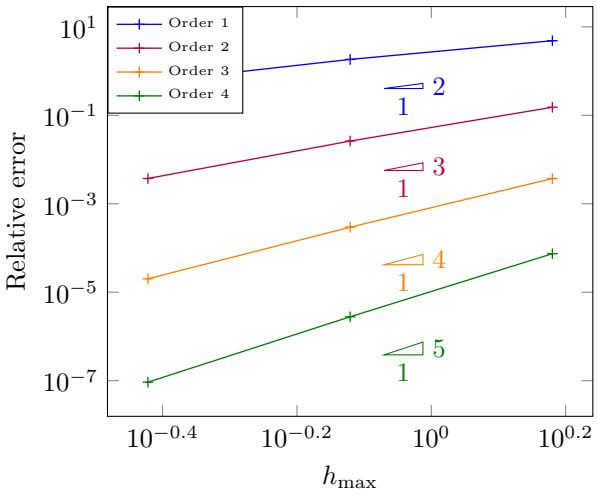

Figure 4: Convergence curves of HDG method (component $\mathbf{u}_x$)

We have also observed that for some stabilization parameters, the method returns accurate results but with a reduced order of convergence. This is in particular the case with no stabilization parameters (see figure 5). Moreover, depending on the stabilization parameters, some fields keep an optimal order of convergence, while it is decreased for others. Theses cases are detailed in table 4.

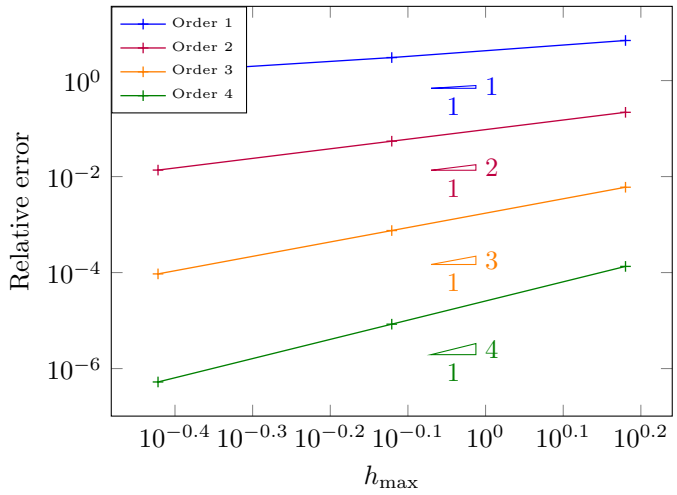

Figure 5: Convergence curves of HDG method with no stabilization parameters (on $\mathbf{u}_x$).

Stabilization parameters (γ_1, γ_2, γ_3, γ_4)	1111	1110	1011	1010	0000	0101	0100	0001
$\mathbf{u}$	$p+1$	$p+1$	$p+1$	$p+1$	p	p	p	p
$\mathbf{w}$	$p+1$	p	$p+1$	$p+1$	p	$p+1$	p	p
$\boldsymbol{\tau}$	$p+1$	$p+1$	p	$p+1$	p	$p+1$	$p+1$	$p+1$
p	$p+1$	$p+1$	p	p	p	$p+1$	$p+1$	p

Table 4: Summary of the convergence order of the HDG method depending on the value of the stabilization parameters, defined in (20).

.

The other combinations of values of the stabilization parameters give deteriorated numerical results, and do not converge. Hence, we have observed that we need the four stabilization parameters to obtain a method with an optimal convergence order. From that, considering the four stabilization parameters to be equal, we investigate the influence of their values on the numerical errors. Figure 6 shows the error of the method function of the stabilization parameters value for order of discretization 3. We observe the same kind of behaviour as in [5, Fig 3.4.7 p.89] for the solid velocity $\mathbf{u}$. Moreover, the relative fluid velocity $\mathbf{w}$ and the pressure p seems to behave in the same way. In Fig. 7, we display the mean relative error of the method. This is calculated as the ratio between the sum of all components ($\mathbf{u}_x$, $\mathbf{u}_y$, $\mathbf{w}_x$, $\mathbf{w}_y$, $\boldsymbol{\tau}_{xx}$, $\boldsymbol{\tau}_{yy}$, $\boldsymbol{\tau}_{xy}$, p) of the L^2 error and the sum of the L^2 norm of the analytical solution. The value of the stabilization parameters seems to be optimal when it is at least 10^3.

6 Conclusion

In this report, we have proposed a numerical method for wave propagation in 2D anisotropic poroelastic media, governed by Biot's model. We have worked in harmonic domain, in order to handle the frequency-dependent parameters. We have chosen to use a HDG method for its flexibility in terms of mesh structure and adaptation, its easy parallelization, its optimal convergence order and all this with a considerably reduced number of degrees of freedom compared to standard DG methods. The HDG implementation can be decomposed into solving a local problem set in a cell of the mesh and a global system having an hybrid variable. We provide a full description of the numerical algorithm including the different steps required for its development. Then, we have validated the HDG method by comparing our results with analytic solutions that have been constructed in a

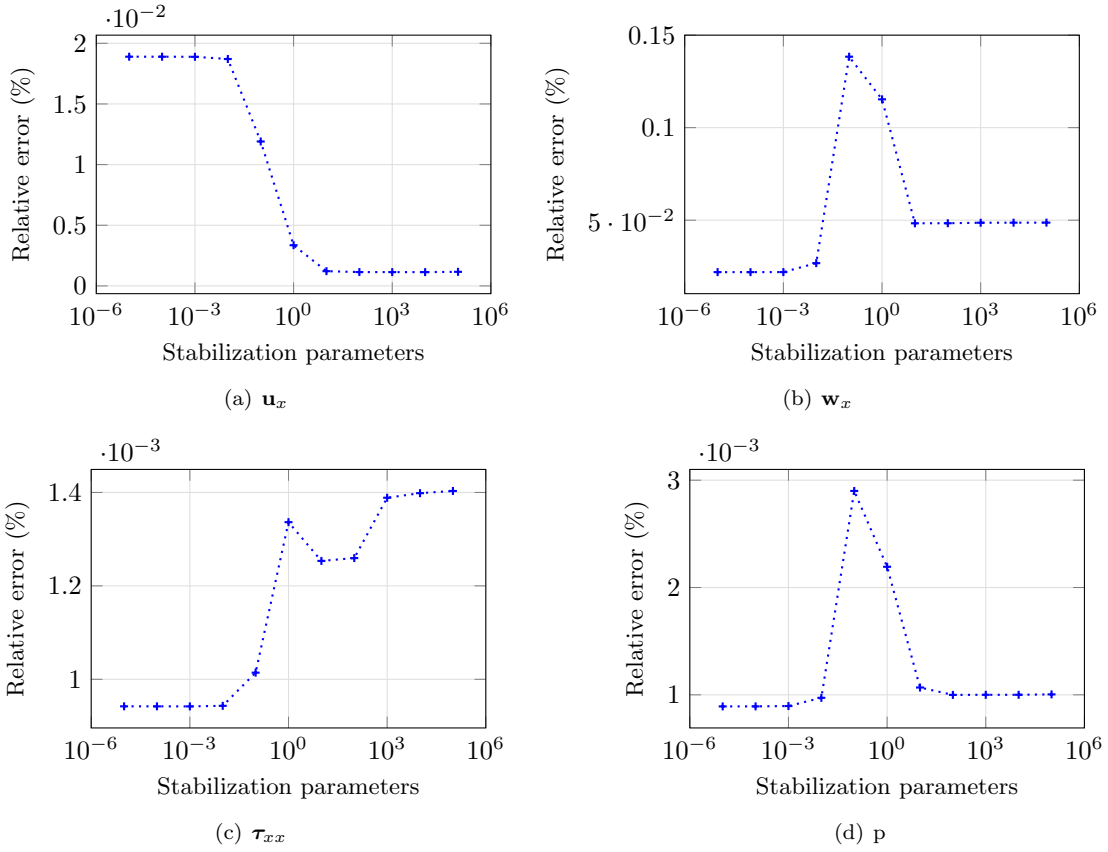

Figure 6: Relative error of HDG method (%) depending on the stabilization parameters in semi-log scale.

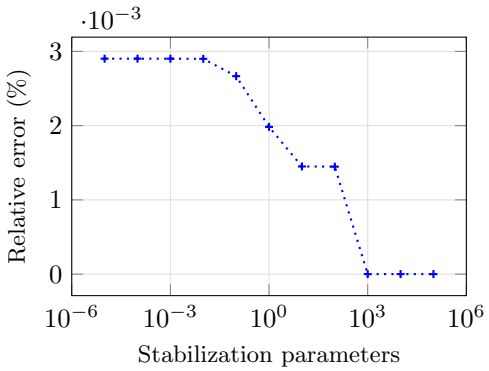

Figure 7: Mean relative error (%) of the HDG method, depending on the stabilization parameters in semi-log scale.

previous work. In particular, we have investigated the convergence of the method depending on the parameters used in the discretization. We have shown that our method keeps an optimal order of convergence with the use of the four parameters.

These results are one of the pillar of CHICkPEA project. They require some additional contributions which are ongoing. For instance, we are currently addressing the well-posedness of the local problem which is at the heart of the HDG formulation. At first glance, we get the well-posedness providing the cell is small enough regarding the characteristic wavelength of the problem. We are also developing non reflecting boundary conditions which are mandatory to truncate the computational domain. Once all of these objectives are achieved, we will consider the HDG formulation for simulating seismokinetic effects.

Contents

References

[1] H. Barucq, J. Diaz, R.-C. Meyer, and H. Pham, *Analytic solutions and transmission eigenvalues in isotropic poroelasticity for bounded domain, scattering of obstacles and fluid-solid interaction problems in 2D*, PhD thesis, INRIA Bordeaux; UPPA (LMA-Pau), 2019.

[2] Biot, *General theory of three-dimensional consolidation*, Journal of Applied Physics, 12, (1941).

[3] ——, *General solutions of the equations of elasticity and consolidation for a porous material*, Journal of Applied Mechanics, (1956).

[4] E. Blanc, *Time-domain numerical modeling of poroelastic waves: the Biot-JKD model with fractional derivatives*, PhD thesis, Aix-Marseille Université, 2013.

[5] M. Bonnasse-Gahot, *High order discontinuous Galerkin methods for time-harmonic elastodynamics*, PhD thesis, 2015.

[6] M. Bonnasse-Gahot, H. Calandra, J. Diaz, and S. Lanteri, *Hybridizable discontinuous Galerkin method for the 2-D frequency-domain elastic wave equations*, Geophysical Journal International, 213 (2018), pp. 637–659.

[7] C. Bordes, L. Jouniaux, S. Garambois, M. Dietrich, J.-P. Pozzi, and S. Gaffet, *Evidence of the theoretically predicted seismo-magnetic conversion*, Geophysical Journal International, 174 (2008), pp. 489–504.

[8] J. Carcione, J. Santos, and S. Picotti, *Anisotropic poroelasticity and wave-induced fluid flow: harmonic finite-element simulations*, Geophysical Journal International, 186 (2011), pp. 1245–1254.

[9] B. Cockburn, B. Dong, J. Guzmán, M. Restelli, and R. Sacco, *A hybridizable discontinuous Galerkin method for steady-state convection-diffusion-reaction problems*, SIAM Journal on Scientific Computing, 31 (2009), pp. 3827–3846.

[10] G. Dazel, *Discontinuous Galerkin methods for poroelastic materials*, Acoustical Society of America, (2013).

[11] J. de la Puente, M. Dumbser, M. Käser, and H. Igel, *Discontinuous Galerkin methods for wave propagation in poroelastic media*, Geophysics, 73 (2008), pp. T77–T97.

[12] M. Dumbser, D. S. Balsara, E. F. Toro, and C.-D. Munz, *A unified framework for the construction of one-step finite volume and discontinuous Galerkin schemes on unstructured meshes*, Journal of Computational Physics, 227 (2008), pp. 8209–8253.

[13] B. Dupuy, L. De Barros, S. Garambois, and J. Virieux, *Wave propagation in heterogeneous porous media formulated in the frequency-space domain using a discontinuous galerkin method*, Geophysics, 76 (2011), pp. N13–N28.

[14] A. Ezziani, *Modélisation mathématique et numérique de la propagation d'ondes dans les milieux viscoélastiques et poroélastiques*, PhD thesis, ENSTA ParisTech, 2005.

[15] G. Fu, *A high-order HDG method for the Biots consolidation model*, Computers & Mathematics with Applications, 77 (2019), pp. 237–252.

[16] S. Garambois, *Etudes expérimentales et théoriques des conversions d'ondes sismo-électriques dans les milieux poreux superficiels*, PhD thesis, 1999.

[17] S. Garambois and M. Dietrich, *Seismoelectic wave conversions in porous media: Field measurements and transfer function analysis.*, Geophysics, (2001).

[18] S. Garambois and M. Dietrich, *Full waveform numerical simulations of seismoelectromagnetic wave conversions in fluid-saturated stratified porous media*, Journal of geophysical research, (2002).

[19] R. P. Gilbert and M. Shoushani, *The Biot model for anisotropic poro-elastic media: The viscoelastic fluid case*, Journal of Computational Acoustics, 25 (2017), p. 1750012.

[20] Haartsen and Pride, *Electroseismic waves from point sources in layered media*, Journal of American Geophysical Union, (1997).

[21] A. Hungria, *Using HDG+ to Compute Solutions of the 3D Linear Elastic and Poroelastic Wave Equations*, PhD thesis, University of Delaware, 2019.

[22] S. Imperiale and P. Joly, *Mathematical and numerical modelling of piezoelectric sensors*, ESAIM: Mathematical Modelling and Numerical Analysis, 46 (2012), pp. 875–909.

[23] R. M. Kirby, S. J. Sherwin, and B. Cockburn, *To CG or to HDG: a comparative study*, Journal of Scientific Computing, 51 (2012), pp. 183–212.

[24] G. I. Lemoine, M. Y. Ou, and R. J. LeVeque, *High-resolution finite volume modeling of wave propagation in orthotropic poroelastic media*, SIAM Journal on Scientific Computing, 35 (2013), pp. B176–B206.

[25] L. Li, S. Lanteri, and R. Perrussel, *Numerical investigation of a high order hybridizable discontinuous Galerkin method for 2D time-harmonic Maxwell's equations*, COMPEL-The international journal for computation and mathematics in electrical and electronic engineering, (2013).

[26] X. LI, D. Yao, and R. W. Lewis, *A discontinuous Galerkin finite element method for dynamic and wave propagation problems in non-linear solids and saturated porous media*, International journal for numerical methods in engineering, (2002).

[27] C. Morency and J. Tromp, *Spectral-element simulations of wave propagation in porous media*, Geophysical Journal International, 175 (2008), pp. 301–345.

[28] S. Pride, *Governing equations for the coupled electromagnetics and acoustics of porous media*, Physical Review B, 50 (1994), p. 15678.

[29] S. R. Pride, *Relationships between seismic and hydrological properties*, in Hydrogeophysics, Springer, 2005, pp. 253–290.

[30] J. Puente, M. Dumbser, M. Kser, and H. Igel, *Discontinuous Galerkin methods for wave propagation in poroelastic media*, Geophysics, (2008).

[31] M. Schanz, *Wave propagation in viscoelastic and poroelastic continua: a boundary element approach*, vol. 2, Springer Science & Business Media, 2012.

[32] Q. Serra, M. Ichchou, and J.-F. Deü, *Wave properties in poroelastic media using a wave finite element method*, Journal of Sound and Vibration, 335 (2015), pp. 125–146.

[33] K. Shukla, J. S. Hesthaven, J. M. Carcione, R. Ye, J. de la Puente, and P. Jaiswal, *A nodal discontinuous Galerkin finite element method for the poroelastic wave equation*, Computational Geosciences, 23 (2019), pp. 595–615.

[34] S.-C. Soon, B. Cockburn, and H. K. Stolarski, *A hybridizable discontinuous Galerkin method for linear elasticity*, International journal for numerical methods in engineering, 80 (2009), pp. 1058–1092.

[35] N. D. Ward, T. Lähivaara, and S. Eveson, *A discontinuous Galerkin method for poroelastic wave propagation: The two-dimensional case*, Journal of Computational Physics, 350 (2017), pp. 690–727.

[36] S. Warden, S. Garambois, L. Jouniaux, D. Brito, P. Sailhac, and C. Bordes, *Seismoelectric wave propagation numerical modelling in partially saturated materials*, Geophysical Journal International, 194 (2013), pp. 1498–1513.

[37] F. Wenzlau and T. M. Müller, *Finite-difference modeling of wave propagation and diffusion in poroelastic media*, Geophysics, 74 (2009), pp. T55–T66.

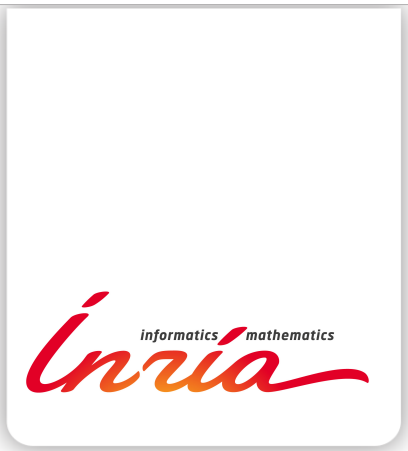

RESEARCH CENTRE
BORDEAUX – SUD-OUEST

200 avenue de la Vieille Tour
33405 Talence Cedex

Publisher
Inria
Domaine de Voluceau - Rocquencourt
BP 105 - 78153 Le Chesnay Cedex
inria.fr

ISSN 0249-6399